*Article*

# Leveraging Elasticity to Uncover the Role of Rabinowitsch Suspension through a Wavelike Conduit: Consolidated Blood Suspension Application

Sara I. Abdelsalam [1,2,]* and Abdullah Z. Zaher [3]

[1] Basic Science, Faculty of Engineering, The British University in Egypt, Al-Shorouk City, Cairo 11837, Egypt
[2] Instituto de Matemáticas—Juriquilla, Universidad Nacional Autónoma de México, Blvd. Juriquilla 3001, Querétaro 76230, Mexico
[3] Engineering Mathematics and Physics Department, Faculty of Engineering, Shubra-Benha University, Cairo 11629, Egypt; abdullah.zaher@feng.bu.edu.eg
* Correspondence: sara.abdelsalam@bue.edu.eg or siabdelsalam@im.unam.mx

**Abstract:** The present work presents a mathematical investigation of a Rabinowitsch suspension fluid through elastic walls with heat transfer under the effect of electroosmotic forces (EOFs). The governing equations contain empirical stress-strain equations of the Rabinowitsch fluid model and equations of fluid motion along with heat transfer. It is of interest in this work to study the effects of EOFs, which are rigid spherical particles that are suspended in the Rabinowitsch fluid, the Grashof parameter, heat source, and elasticity on the shear stress of the Rabinowitsch fluid model and flow quantities. The solutions are achieved by taking long wavelength approximation with the creeping flow system. A comparison is set between the effect of pseudoplasticity and dilatation on the behaviour of shear stress, axial velocity, and pressure rise. Physical behaviours have been graphically discussed. It was found that the Rabinowitsch and electroosmotic parameters enhance the shear stress while they reduce the pressure gradient. A biomedical application to the problem is presented. The present analysis is particularly important in biomedicine and physiology.

**Keywords:** elasticity; electroosmotic forces; heat transfer; Rabinowitsch fluid; suspension

## 1. Introduction

The movement of blood liquids is an important study for the mathematical simulation of medical applications. Rabinowitsch fluid is one of the fluids that simulate blood movement because the Rabinowitsch model effectively relies on studying the result of lubricant additives, for a wide range of shear rates, and studying their experimental data. Over the past decades, scientists have made active efforts to increase the ability of solidifying the features of non-Newtonian lubricants using long-chain quantities by adding a very small addition of the polymer solution. A very important result from this is that this result reduces the lubricant sensitivity. Additionally, a non-linear relationship appears between the shear stress rate and shear pressure. Through those recent actions based on the Rabinowitsch model, Akbar and Butt [1] studied the flow of the Rabinowitsch model due to the cilia located on the wall. Moreover, Singh et al. [2] studied the movement of Rabinowitsch fluid through peristaltic flow. In addition, Vaidya [3] investigated the movement of Rabinowitsch fluid through the oblique wall of a channel, while Sadaf and Nadeem [4] studied the Rabinowitsch model through a non-uniform conduit with peristalsis. Choudhari et al. [5] also studied the effect of slipping on the oscillating transmission of a Rabinowitsch model in a non-uniform channel.

In recent years, microfluidic systems have been developed through the use of Electric-Double-Layer (EDL). This increased interest is reflected in references [6–8]. Electrical osmosis is defined as the movement of a liquid in relation to a fixed surface due to the

presence of an externally applied electric field. One of the first studies that have studied the application of these external forces is by Ross [9]. The idea is that electrical ripening comes into contact with the aqueous electrolytic solution with the solids and then generates a relatively electrical charge. In addition, the opposite ion charge is attracted to that charge on the surface and the opposite process from the ions on the surface and shows the double layer, and thus, the surface becomes electrically charged. As a result of this phenomenon, a process of acceleration of the liquid by migrating ions occurs, and the resulting flow is called electromagnetic flow.

The study of the movement of suspended particles inside the fluid is considered the most important medical application. The movement of the fluid that contains particles is similar to the movement of the blood plasma since the blood consists of solid materials, that is, it is a liquid in which those substances swim. In that sense, there are a lot of species studied such as sickle cell (Hb SS), plasma cell dyscrasias, normal blood, controlled hypertension, uncontrolled hypertension, and polycythaemia. Each of these types is known by a specific haematocrit, i.e., $C = 0.248$, $C = 0.28$, $C = 0.426$, $C = 0.4325$, $C = 0.4331$, and $C = 0.632$ [10]. In addition, the study of the movement of suspended particles inside fluids is very interesting because they resemble white blood cells, red blood cells, and/or platelets that move inside the blood. Many experimental and analytical studies have focused on studying suspended particles because of their great importance in improving and understanding the blood flow and the distribution of proteins within it [11–13].

The geometrical shape of fluid flow has an important role in understanding various properties of different fluid flows such as blood flow and other important applications. Most studies that have discussed fluid movement have relied on solid ducts and tubes [14–24]. Because biological flows depend on their flexible flow fields, and this appears through their flexible nature, the flow and the movement of Newtonian and non-Newtonian fluids through walls of a flexible nature carry many important medical applications such as blood flow through the arteries, small blood vessels, heart systems, and others, which, according to some studies, revealed that the velocity of the blood is greatly affected by the elastic placement of the walls. Some of the work that has been interested in discussing the flow rate through elastic nature can be found in the refs. [25–31].

Accordingly, this work attempts to fill the void of the movement of the particulate suspension under the effects of electroosmotic forces using Rabinowitsch fluid. Analytical solution is used to obtain the physical parameters of the problem subjected to appropriate boundary conditions. The impact of relevant parameters is discussed graphically.

## 2. The Mathematical Model and the Rabinowitsch Fluid Equation

Consider a particulate suspension swimming in a Rabinowitsch fluid through elastic peristaltic walls of a channel with amplitude $a$ and half width $b$. In addition, consider that the deformation on the wall is $\alpha$ as shown in Figure 1. Furthermore, the inlet pressure is defined as $p_i$ and the outlet pressure is defined as $p_o$, as shown in Figure 1. The effect of the electroosmotic forces on the Rabinowitsch fluid through the elastic peristaltic walls is taken into account. The velocity of the particulate suspension and Rabinowitsch fluid are denoted by $\vec{V}\left(\overline{U}_p, \overline{V}_p\right)$, $\vec{V}\left(\overline{U}_f, \overline{V}_f\right)$. The mathematical geometry of the channel wall is given by

$$H(\overline{X}, t) = \pm\left(d + a\sin\frac{2\pi}{\lambda}\left(\overline{X} - c\,t\right)\right), \tag{1}$$

Here, $d$ is the radius of the artery channel, $a$ is the amplitude of the wall, $\lambda$ is the amplitude of the peristaltic wave, and $c$ is the blood velocity.

The isotropic rheological equation of a Rabinowitsch fluid takes the following form:

$$\overline{\tau}_{\overline{XY}} + \mu_o\overline{\tau}_{\overline{XY}}^{\ 3} = \mu_S(C)\frac{\partial\overline{U}}{\partial\overline{Y}}, \tag{2}$$

where the coefficient $\mu_o$ represents pseudo-plasticity of the fluid, which takes a fundamental role in determining the nature of fluids; $\mu_S(C)$ is the viscosity of suspension; $\overline{\tau}_{\overline{XY}}$ is the stress tensor; $\overline{U}$ is the velocity component; and $C$ is the volume fraction. The model represents a pseudoplastic state for $\mu_o > 0$, a Newtonian state for $\mu_o = 0$, and an expanded fluid model for $\mu_S < 1$.
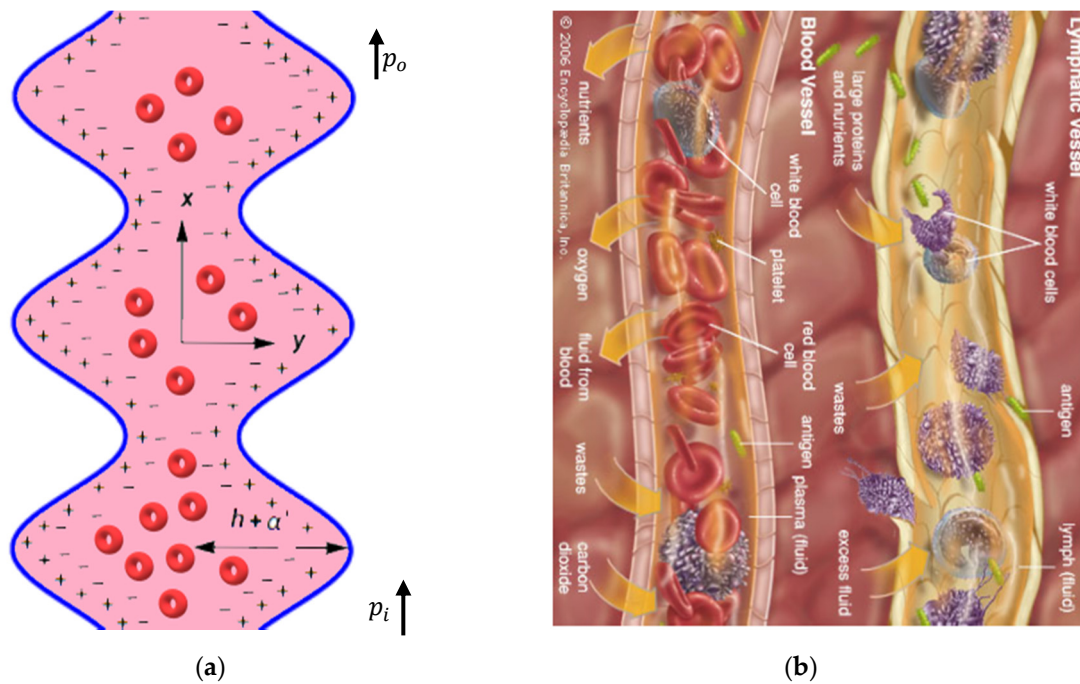


**Figure 1.** (**a**) Physical modelling of the problem. (**b**) Example for extracellular fluid that contains plasma.

The momentum and continuity equations for the problem of both particle and fluid phases are given in the following form [32].

Model of Fluid Phase

$$\frac{\partial \overline{U}_f}{\partial \overline{X}} + \frac{\partial \overline{V}_f}{\partial \overline{Y}} = 0, \tag{3}$$

$$\rho_f\, C_{PH}\left(\frac{\partial \overline{U}_f}{\partial t} + \overline{U}_f \frac{\partial \overline{U}_f}{\partial \overline{X}} + \overline{V}_f \frac{\partial \overline{U}_f}{\partial \overline{Y}}\right)$$
$$= -C_{PH}\frac{\partial \overline{P}}{\partial \overline{X}} + C_{PH}\left[\frac{\partial \tau_{\overline{XX}}}{\partial \overline{X}} + \frac{\partial \tau_{\overline{XY}}}{\partial \overline{Y}}\right] + \rho_e E_x + \rho_f \gamma g\,(T - T_0) - C\,S\left(\overline{U}_f - \overline{U}_P\right), \tag{4}$$

$$\rho_f\, C_{PH}\left(\frac{\partial \overline{V}_f}{\partial t} + \overline{U}_f \frac{\partial \overline{V}_f}{\partial \overline{X}} + \overline{V}_f \frac{\partial \overline{V}_f}{\partial \overline{Y}}\right)$$
$$= -C_{PH}\frac{\partial \overline{P}}{\partial \overline{Y}} + C_{PH}\left[\frac{\partial \tau_{\overline{YX}}}{\partial \overline{X}} + \frac{\partial \tau_{\overline{YY}}}{\partial \overline{Y}}\right] - C\,S\left(\overline{V}_f - \overline{V}_P\right), \tag{5}$$

$$(\rho C)_f\left(\frac{\partial T_f}{\partial t} + \overline{U}_f \frac{\partial T_f}{\partial \overline{X}} + \overline{V}_f \frac{\partial T_f}{\partial \overline{Y}}\right) = k\left(\frac{\partial^2 T}{\partial \overline{X}^2} + \frac{\partial^2 T}{\partial \overline{Y}^2}\right) + H_S, \tag{6}$$

Model of Particle Phase

$$\frac{\partial \overline{U}_P}{\partial \overline{X}} + \frac{\partial \overline{V}_P}{\partial \overline{Y}} = 0, \tag{7}$$

$$\rho_P\, C_{PH}\left(\frac{\partial \overline{U}_P}{\partial t} + \overline{U}_P \frac{\partial \overline{U}_P}{\partial \overline{X}} + \overline{V}_P \frac{\partial \overline{U}_P}{\partial \overline{Y}}\right) = -C_{PH}\frac{\partial \overline{P}}{\partial \overline{X}} + C\,S\left(\overline{U}_f - \overline{U}_P\right), \tag{8}$$

$$\rho_f\, C_{PH}\left(\frac{\partial \overline{V}_P}{\partial t} + \overline{U}_P \frac{\partial \overline{V}_P}{\partial \overline{X}} + \overline{V}_P \frac{\partial \overline{V}_P}{\partial \overline{Y}}\right) = -C_{PH}\frac{\partial \overline{P}}{\partial \overline{Y}} + C\,S\left(\overline{V}_f - \overline{V}_P\right), \tag{9}$$

where $C_{PH} = 1 - C$, $S$ is the drag coefficient and $\mu_S(C)$ is the viscosity of suspension, $\rho_{f,p}$ is the fluid and particle density, $\rho_e$ is the electrical charge density, $E_x$ is the axial electric field, $\gamma$ is the thermal expansion coefficient, g is the gravitational acceleration, $k$ is the thermal conductivity, and $H_S$ is the constant heat absorption or heat generation. The empirical relation for $S$ and $\mu_S(C)$ can be described as

$$\mu_S = 1/(1 - m\,C), \quad m = 0.07 * Exp\left[2.49 * C - \tfrac{1107}{273} * Exp[-1.69 * C]\right],$$
$$S = \tfrac{9\mu_0}{2\in^2}\gamma(C), \quad \gamma(C) = \tfrac{4 + 3\sqrt{8C - 3C^2} + 3C}{(2 - 3C)^2}. \tag{10}$$

Here, $\mu_0$ is the viscosity of fluid for suspending medium, and $\in$ is the radius of a particle.

Now, we use the convenient transformation to convert from fixed frame to wave frame as follows:

$$\overline{x} = \overline{X} - ct, \quad \overline{y} = \overline{Y}, \quad \overline{u} = \overline{U} - c, \quad p = P. \tag{11}$$

Then, the mathematical formulation and Rabinowitsch fluid Equations (1)–(9) take the following form:

Rabinowitsch fluid equation

$$\overline{\tau}_{\overline{xy}} + \mu_o \overline{\tau}_{\overline{xy}}{}^3 = \mu_s(C) \frac{\partial \overline{u}_f}{\partial \overline{y}}, \tag{12}$$

Model of fluid phase

$$\rho_f\, C_{PH}\left(\overline{u}_f \frac{\partial \overline{u}_f}{\partial \overline{x}} + \overline{v}_f \frac{\partial \overline{u}_f}{\partial \overline{y}}\right) \tag{13}$$

$$\rho_f\, C_{PH}\left(\overline{u}_f \frac{\partial \overline{V}_f}{\partial \overline{x}} + \overline{v}_f \frac{\partial \overline{v}_f}{\partial \overline{y}}\right) = -C_{PH}\frac{\partial \overline{p}}{\partial \overline{y}} + C_{PH}\left[\frac{\partial \tau_{\overline{yx}}}{\partial \overline{x}^2} + \frac{\partial \tau_{\overline{yy}}}{\partial \overline{y}^2}\right] - C\,S\left(\overline{v}_f - \overline{v}_P\right), \tag{14}$$

$$(\rho C)_f\left(\frac{\partial T_f}{\partial t} + \overline{u}_f \frac{\partial T_f}{\partial \overline{x}} + \overline{v}_f \frac{\partial T_f}{\partial \overline{y}}\right) = k\left(\frac{\partial^2 T}{\partial \overline{x}^2} + \frac{\partial^2 T}{\partial \overline{y}^2}\right) + H_S, \tag{15}$$

Model of particle phase

$$\rho_P\, C_{PH}\left(\overline{u}_P \frac{\partial \overline{u}_P}{\partial \overline{x}} + \overline{v}_P \frac{\partial \overline{u}_P}{\partial \overline{y}}\right) = -C_{PH}\frac{\partial \overline{p}}{\partial \overline{x}} + C\,S\left(\overline{u}_f - \overline{u}_P\right), \tag{16}$$

$$\rho_f\, C_{PH}\left(\overline{u}_P \frac{\partial \overline{v}_P}{\partial \overline{x}} + \overline{v}_P \frac{\partial \overline{v}_P}{\partial \overline{y}}\right) = -C_{PH}\frac{\partial \overline{p}}{\partial \overline{y}} + C\,S\left(\overline{v}_f - \overline{v}_P\right), \tag{17}$$

### 3. Electroosmotic Flow

The Poisson–Boltzmann equation:

$$\nabla^2 \overline{\varphi} = \frac{\rho_e}{\epsilon}, \tag{18}$$

where $\rho_e$ is a charge density, $\epsilon$ is the electric permittivity, and $\overline{\varphi}$ is the electroosmotic potential function.

The charge density $\rho_e$ of the fluid in a unit volume is given by:

$$\rho_e = \varepsilon\, e\left(n^+ - n^-\right) = -2\varepsilon\, e\, n_0 \sinh\left\{\frac{\varepsilon\, e\overline{\varphi}}{k_B T_{av}}\right\}, \tag{19}$$

$$n^- = n_0\, e^{\frac{\varepsilon\, e\overline{\varphi}}{k_B T_{av}}}, \ n^+ = n_0\, e^{-\frac{\varepsilon\, e\overline{\varphi}}{k_B T_{av}}}, \tag{20}$$

where $\varepsilon$, $n^+$, $n^-$, $e, k_B$, and $T_{av}$ are the valence of ions, the number densities of positive and negative ions, electric charge, Boltzmann's constant, local absolute temperature of the electrolytic solution, and bulk volume concentration of positive or negative ions,

respectively. In addition, using the Debye–Huckel linearisation principle, $\left\{\frac{\epsilon e \varphi'}{k_B T_{av}} \ll 1\right\}$. Equation (19) reduces to

$$\rho_e = \frac{-\epsilon}{\Gamma^2}\,\overline{\varphi}, \tag{21}$$

where $\Gamma = (\epsilon e)^{-1}\sqrt{\frac{\epsilon\,k_B T_{av}}{2\,n_0}}$ is the Debye–Huckel parameter, which describes the properties of the EDL thickness. The solution for the distribution of the electroosmotic potential can easily be achieved using the Poisson–Boltzmann equation:

$$\frac{\partial^2\overline{\varphi}}{\partial\overline{x}^2} + \frac{\partial^2\overline{\varphi}}{\partial\overline{y}^2} = \frac{1}{\Gamma^2}\,\overline{\varphi}, \tag{22}$$

## 4. Non-Dimensional Physical Parameters

The non dimensionless quantities are introduced in the following expression

$$
\begin{gathered}
u_{P,f} = \frac{\overline{u}_{P,f}}{c}, y = \frac{\overline{y}}{a},\, v_{P,f} = \frac{\overline{v}_{P,f}}{\delta c},\, p = \frac{a^2}{\lambda\,c\,\mu_o}\overline{p},\, \delta = \frac{a}{\lambda},\, \vartheta = \frac{\overline{\varphi}}{\zeta},\, Re = \frac{\rho_f\,c\,a}{\mu_0}, \\
Gr = \frac{\rho_f\gamma g\,a^2\,T_0}{\mu_o\,c},\, \theta = \frac{T - T_0}{T_0},\, \overline{\mu} = \frac{\mu_s(C)}{\mu_0},\, \tau = \frac{a}{c\mu_0}\overline{\tau},\, U_{HS} = -\frac{E_x\,\epsilon\,\zeta}{\mu_0\,c}, \\
K = \frac{\mu_S\,(C)c^2\mu_0^2}{a^2},\, m = \frac{a}{k^2},\, M = \frac{Sa^2}{\mu_S\,(C)(1-C)},\, Q = \frac{H_s a^2}{\mu_0\,T_o},\, p_r = \frac{\mu_o C_f}{k}, \\
h = \frac{H}{d},\, \phi = \frac{a}{d}
\end{gathered}
\tag{23}
$$

where $K$, $m$, $Q$, $p_r$, $U_{HS}$, $Gr$, and $Re$ are, respectively, the Rabinowitsch fluid parameter, electroosmotic parameter, heat source, Prandtl number, electroosmotic velocity, Grashof number, and Reynolds number. The non-dimensional formulation of the mathematical geometry for the channel wall is given by

$$h(x) = \pm(1 + \phi\sin 2\pi\,x),$$

where $\phi$ is the amplitude ratio.

After using the non-dimensional physical parameters given by Equation (23) in the governing Equations (12)–(17) and in Equation (22), we find:

Non-dimensional Rabinowitsch fluid equations

$$\tau_{xy} + K\,{\tau_{xy}}^3 = \overline{\mu}\frac{\partial u_f}{\partial y}, \tag{24}$$

Non-dimensional model of fluid phase

$$R_e\,\delta\,C_{PH}\left(u_f\frac{\partial u_f}{\partial x} + v_f\frac{\partial u_f}{\partial y}\right) = -C_{PH}\frac{\partial p}{\partial x} + C_{PH}\left[\delta\frac{\partial\tau_{xx}}{\partial x} + \frac{\partial\tau_{xy}}{\partial y}\right] + m^2 U_{HS}\cosh my + G_r\,(T - T_0) - C\,C_{PH}\,\overline{\mu}\,M\left(u_f - u_P\right), \tag{25}$$

$$R_e\,\delta\,C_{PH}\left(u_f\frac{\partial v_f}{\partial x} + v_f\frac{\partial v_f}{\partial y}\right) = -C_{PH}\frac{\partial p}{\partial y} + C_{PH}\left[\frac{\partial\tau_{yx}}{\partial x} + \frac{\partial\tau_{yy}}{\partial y}\right] - C\,C_{PH}\,\overline{\mu}\,M\left(v_f - v_P\right), \tag{26}$$

$$R_e\,p_r\delta\left(u_f\frac{\partial\theta}{\partial x} + v_f\frac{\partial\theta}{\partial y}\right) = \left(\frac{\partial^2\theta}{\partial x^2} + \frac{\partial^2\theta}{\partial y^2}\right) + Q, \tag{27}$$

Non-dimensional model of particle phase

$$\frac{\rho_P}{\rho_f}\,CR_e\delta\left(u_P\frac{\partial u_P}{\partial\overline{x}} + v_P\frac{\partial u_P}{\partial\overline{y}}\right) = -C\frac{\partial p}{\partial x} + C\,C_{PH}\,\overline{\mu}\,M\,\left(u_f - u_P\right), \tag{28}$$

$$\frac{\rho_P}{\rho_f}\,CR_e\delta\left(u_P\frac{\partial v_P}{\partial x} + v_P\frac{\partial v_P}{\partial y}\right) = -C\frac{\partial p}{\partial y} + C\,C_{PH}\,\overline{\mu}\,M\,\delta\left(v_f - v_P\right), \tag{29}$$

with dimensionless boundary conditions

$$
\begin{array}{cccccc}
u = -1, & \theta = 0, & \vartheta = 1 & \text{at} & y = h(x), \\
u = -1, & \theta = 0, & \vartheta = 1 & \text{at} & y = -h(x) \\
& \tau_{xy} = 0 \; at \; y = 0.
\end{array}
\tag{30}
$$

## 5. Methodology

Taking a long wavelength approximation and a creeping flow system, i.e., $\delta \ll 1$, the solution of Equations (24)–(29) takes the following form

$$
\theta(y) = \frac{1}{2}Q(h-y)(h+y),
\tag{31}
$$

$$
\tau_{xy} = \frac{6\,P\,y + G_r\,Q\,y\left(-3h^2+y^2\right) - 6\,m\,U_{HS}\,\frac{sinh\,(my)}{cosh\,(mh)}}{6\,C_{PH}},
\tag{32}
$$

$$
\begin{aligned}
u(y) = c_0\{ & c_1 + c_2\,y^{10} + c_3\,y^2 + c_4\,y^8 + c_5\,y^6 + c_6\,Cosh(3my) + c_7\,y\,Sinh(2my) + c_8\,P_1(y) \\
& + Cosh(2my)(c_9 + c_{10}\,P_2(y)) + y\,Sinh(my)(c_{16} + c_{12}\,P_1(y)P_2(y) + c_{13}\,P_3(y)) + c_{17} \\
& + Cosh(my)(c_{18} + c_{19}\,P_4(y) + c_{20}\,y^4 + c_{21}\,y^2 + (c_{23} - c_{14}\,y^2(P_1(y))^2))\}.
\end{aligned}
\tag{33}
$$

where $P$, $P_j$ ($j = 1 \to 4$) and the constants $c_i$ ($i = 1 \to 23$) are given in the Appendix A.

## 6. Theoretical Determination of Pressure Gradient and Pressure Rise Application in Blood Flows

In this section, the deformation in the walls that is defined by elasticity in the channel walls is taken into account, which appears from the pressure shown in Figure 1. According to Rubinow and Keller [28], the flow rate and pressure gradient are related by the following expression:

$$
Q = -\sigma(p_i - p_o)\frac{\partial p}{\partial x},
\tag{34}
$$

The flow rate is defined as

$$
Q = \int_0^h u(y)dy,
\tag{35}
$$

Following the hypothesis of elastic walls, according to Rubinow and Keller [28], and using Equations (33)–(35), it is found that the flow rate takes the following form as follows

$$
Q = \sigma_1(p_i - p_o)\left(-\frac{\partial p}{\partial x}\right)^3 + \sigma_2(p_i - p_o)\left(-\frac{\partial p}{\partial x}\right)^2 + \sigma_3(p_i - p_o)\left(-\frac{\partial p}{\partial x}\right) + c_{24}
\tag{36}
$$

such that $c_{24}$ is given in the Appendix A.

Where

$$
\sigma_1(p_i - p_o) = \frac{\alpha(x)^5 k}{5A\,M^3},
\tag{37}
$$

$$
\begin{aligned}
\sigma_2(p_i - p_o) = \quad & \frac{1}{8640\overline{\mu}\,m^6 M^3}\Big( \frac{13824}{7}G_r\,\alpha(x)^7\,K\,m^6 Q + 103680\;\alpha(x)K\,m^4\,U_{HS} \\
& + 25920\,\alpha(x)K\,m^4(2 + \alpha(x)^2 m^2)\,Uhs - 155520\,K\,m^3\,U_{HS}\,tanh\,(\alpha(x)m) \\
& - 77760\,\alpha\,(x)^2\,K\,m^5\,U_{HS}\,tanh(\alpha(x)m)\Big),
\end{aligned}
\tag{38}
$$

$$
\begin{aligned}
\sigma_3(p_i - p_o) = {}& \tfrac{1}{8640\overline{\mu}\, m^6 M^3} \Big( -2880\ \alpha(x)^3 m^6 M^2 - \tfrac{5312}{7} G_r{}^2\ \alpha(x)^9 K m^6 Q^2 \\
& +4320\ \alpha(x)^3 K m^8 U_{HS}{}^2 sech^2(\alpha(x)m)) + 414720\ G_r\ \alpha(x)\ K\ Q\ U_{HS} \\
& -17280\ G_r\ \alpha(x)^3 K\ m^4 Q\ U_{HS} + 17280\ G_r\ \alpha(x)\ K\ m^2\ (24 - \alpha(x)^2 m^2)\ Q\ U_{HS} \\
& -17280\ G_r\ \alpha(x)\ K m^2 (-12 - 3\,\alpha(x)^2 m^2 + \alpha(x)^4 m^4)\ Q\ U_{HS} \\
& +6480\ \ \alpha(x)\ K\ m^6\ U_{HS}{}^2 sech(\alpha(x)m)sinh(\alpha(x)m) - 622080\ \ G_r\ K\ m\ Q\ U_{HS}\ tanh(\alpha(x)m) \\
& -103680\, G_r\ \alpha(x)^2 K\ m^3\ Q\ U_{HS}\ tanh(\alpha(x)m) + 17280\, G_r\ \alpha(x)^4\ K\ m^5\ Q\ U_{HS}\ tanh(\alpha(x)m) \\
& +17280\ G_r\ \alpha(x)^2 K\ m^3\ (-12 + \alpha(x)^2 m^2)\ Q\ U_{HS}\ tanh(\alpha(x)m) \\
& -51840\ \ G_r\ K\ m\ (8 + \alpha(x)^2 m^2)\ Q\ U_{HS}\ tanh(\alpha(x)m) \\
& -3240\ \ K\ m^5\ U_{HS}{}^2\ sech(\alpha(x)m)sinh(\alpha(x)m) \\
& -6480\ \alpha(x)^2\ K\ m^7 U_{HS}\ sech(\alpha(x)m)sinh(\alpha(x)m) \Big),
\end{aligned}
\tag{39}
$$

Here, $\alpha(x) = h(x) + \alpha'$, where $h(x)$ and $\alpha'$ are the radii of the channel for peristalsis and elasticity, respectively. Additionally, the pressure rise is defined as

$$
\Delta p = \int_0^1 \left( \frac{dp}{dx} \right) dx.
\tag{40}
$$

## 7. Graphical Results and Discussion

The goal of this section is to study the effect of the pertinent parameters on the resulted physical expression. In doing so, the Mathematica program is used in order to investigate the impact of Rabinowitsch parameter $K$, Prandlt number $Pr$, heat source $Q$, electroosmotic parameter $m$, volume fraction $C$, Grashof number $Gr$, maximum electroosmotic velocity $U_{HS}$, and radius of the channel for elasticity $\alpha'$ on the shear stress $\tau_{xy}$, axial velocity $U(y)$, pressure gradient $\frac{dp}{dx}$, and pressure rise $\Delta p$. A graphical comparison is also set to compare between pseudoplastic and dilatant fluids.

Figures 2–9 are plotted to investigate the impact of $U_{HS}$, $C$, $Gr$, $m$, $K$, and $\alpha'$ on $\tau_{xy}$ for sundry values of the parameters of interest. It is observed from Figures 2–7 that the Rabinowitsch shear stress improves prominently with increasing all the parameters, even with increasing the curviness of the conduit in both the lower and upper halves of the channel. Figures 8 and 9 demonstrate a comparison between the impact of pseudoplasticity and dilatation on the shear stress profile through $x$ and $y$ axes, respectively. It is notable from the latter figures that for pseudoplastic fluid, $\tau_{xy}$ is enhanced along the conduit through the $x$-axis, whereas for the case of dilatant fluids, a reverse effect is observed. It is also seen that $\tau_{xy}$ behaves differently along the $y$-axis where it is seen that, for the pseudoplastic fluids, $\tau_{xy}$ decays near the lower wall of the channel and improves with an increase in the curviness of the channel. An exact opposite behaviour is seen for dilatant fluids, as seen in Figure 9.

Figures 10–16 illustrate the impact of $K$, $U_{HS}$, $Gr$, $C$, $m$, and $\alpha'$ on $U(y)$ for various values of the pertinent parameters. It is noticed that $K$, $U_{HS}$, and $\alpha'$ play a distinguished role in lessening the fluid velocity, as seen in Figures 10, 11 and 15. It is also depicted that $Gr$, $C$, and $m$ disturb the velocity profile significantly, as observed in Figures 12–14. It is noticed that the latter parameters barely have an effect on $U(y)$ near the walls of the channel, whereas they enhance the flow in the centre part of the channel. It is generally noticed that $U(y)$ has a parabolic shape along the conduit for all the parameters under consideration. Figure 16 is plotted to spot the difference in the behaviour of $U(y)$ for pseudoplastic and dilated fluids. It is demonstrated that for pseudoplastic fluids, $U(y)$ is not disturbed at all near the walls of the conduit, whereas it is noticed that for dilated fluids, the flow is decelerated at the centre of the channel.
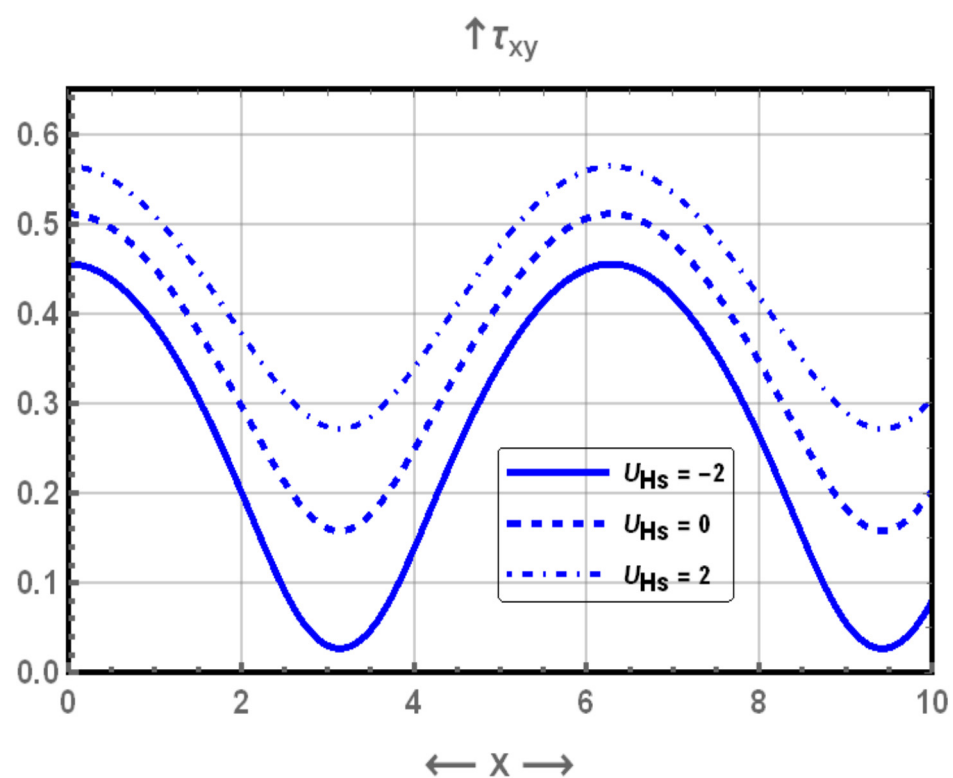
**↑ $\tau_{xy}$**



**Figure 2.** Display of shear stress profile for different values of $U_{HS}$.
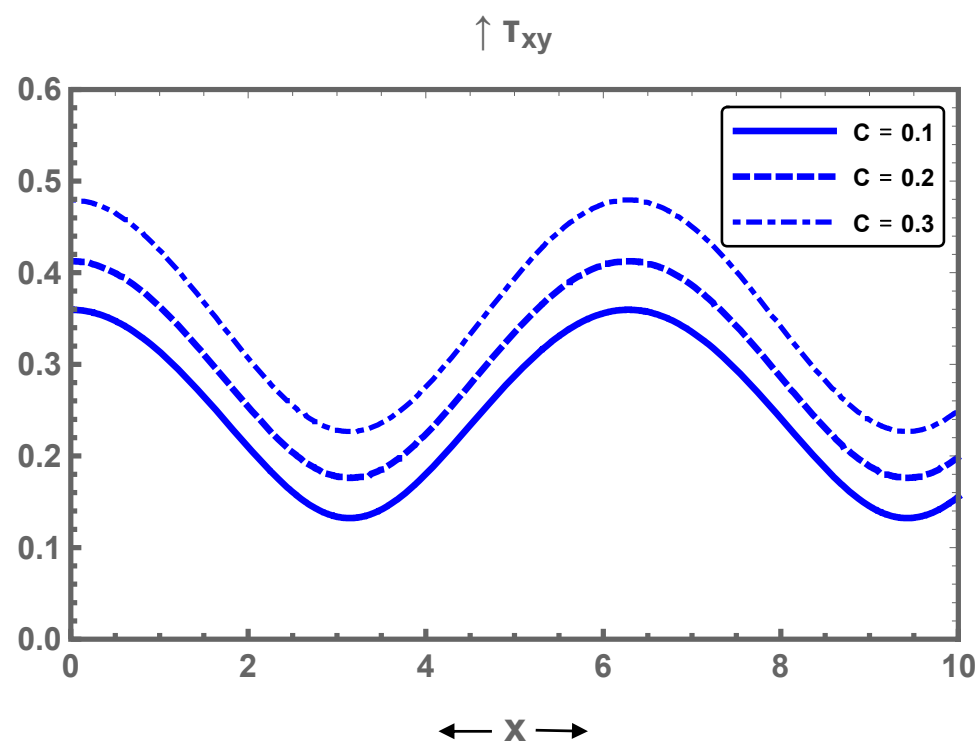
**↑ T$_{xy}$**



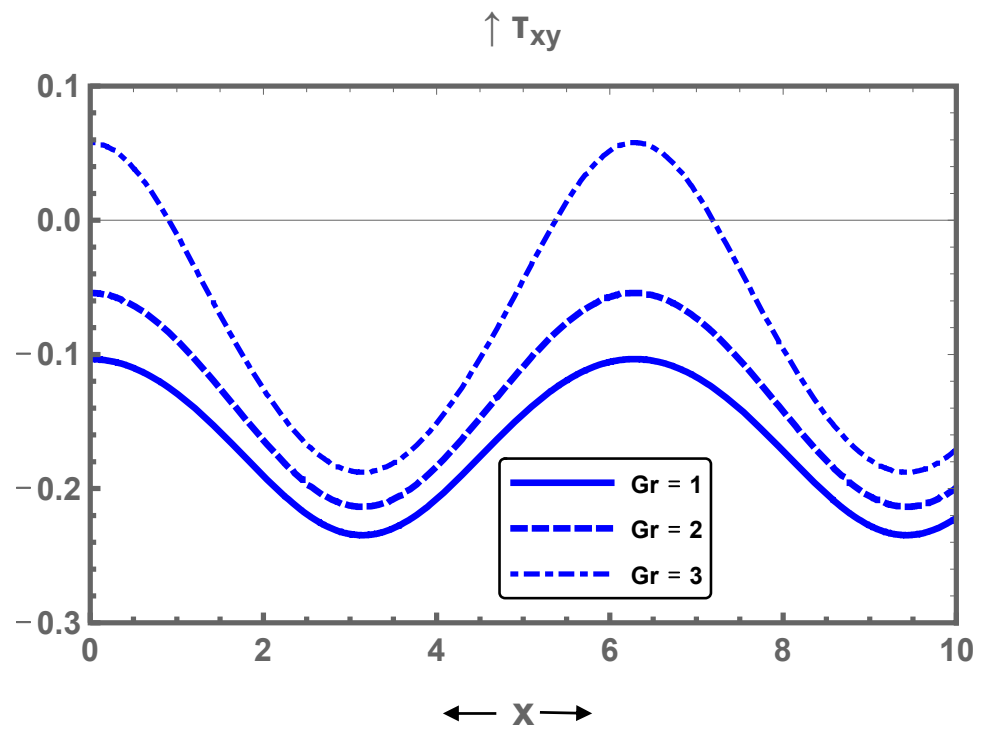**Figure 3.** Display of shear stress profile for different values of *C*.

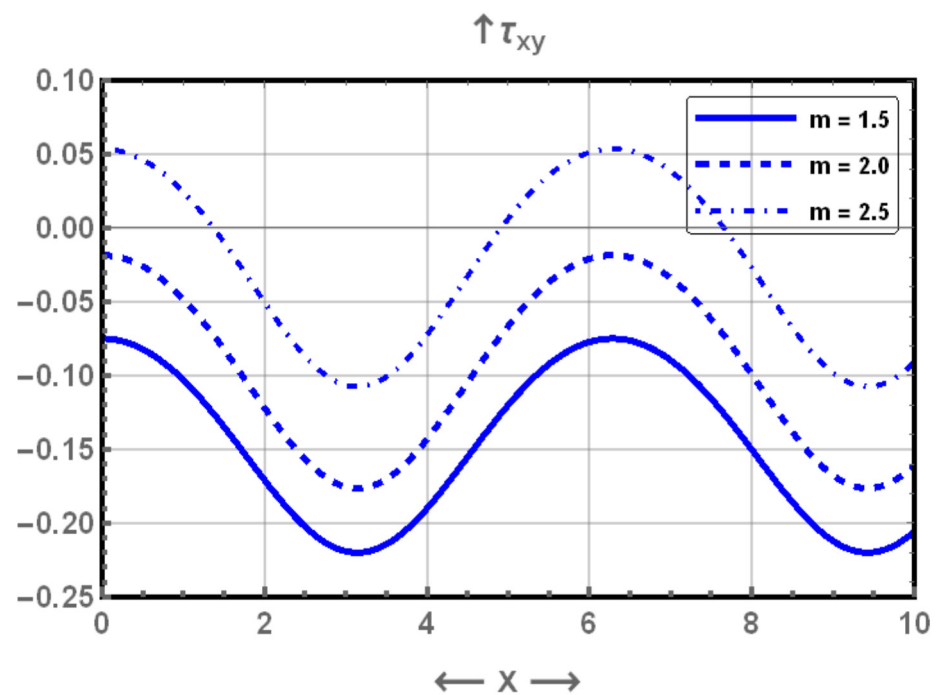**Figure 4.** Display of shear stress profile for different values of *Gr*.

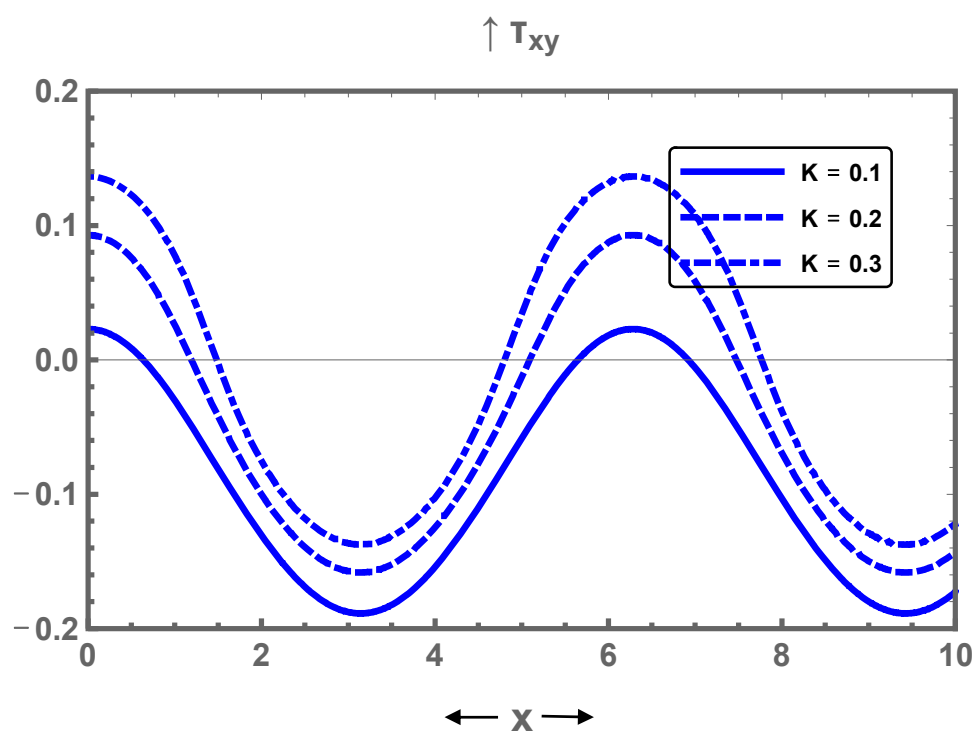**Figure 5.** Display of shear stress profile for different values of *m*.

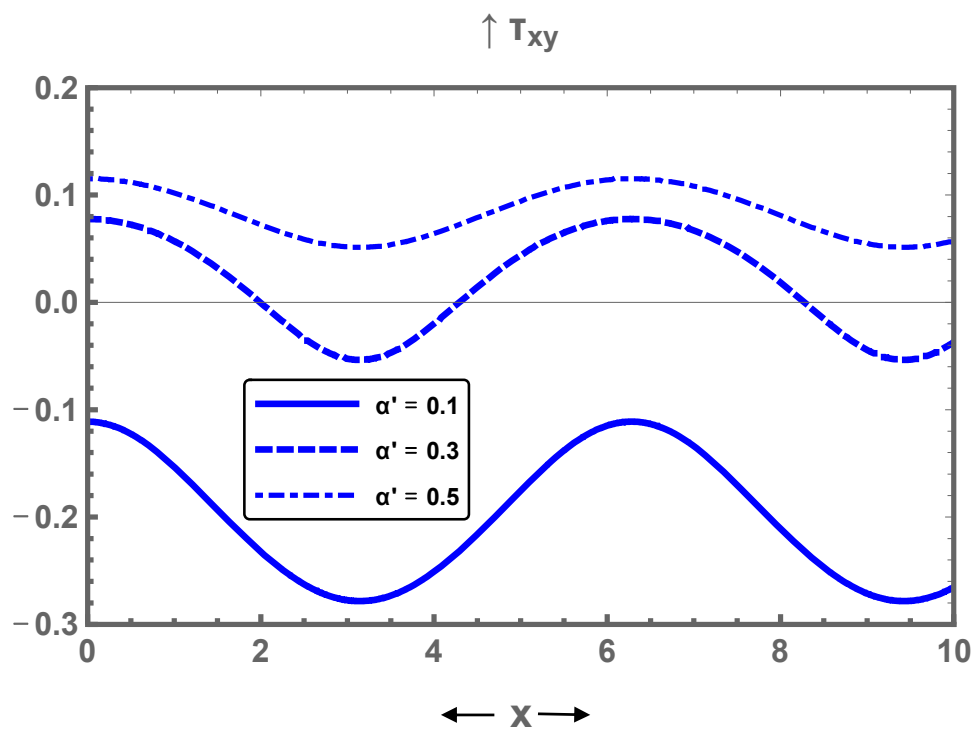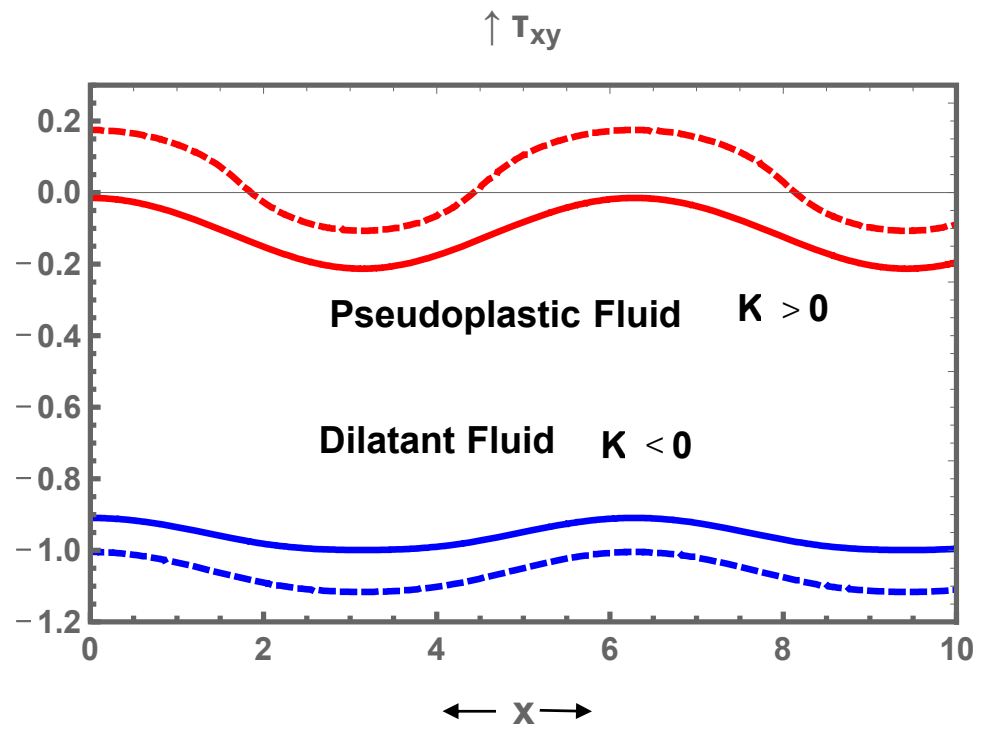**Figure 6.** Display of shear stress profile for different values of *K*.



**Figure 7.** Display of shear stress profile for different values of $\alpha'$.

**Figure 8.** Display of shear stress profile via *x* for pseudoplastic and dilatant fluids.
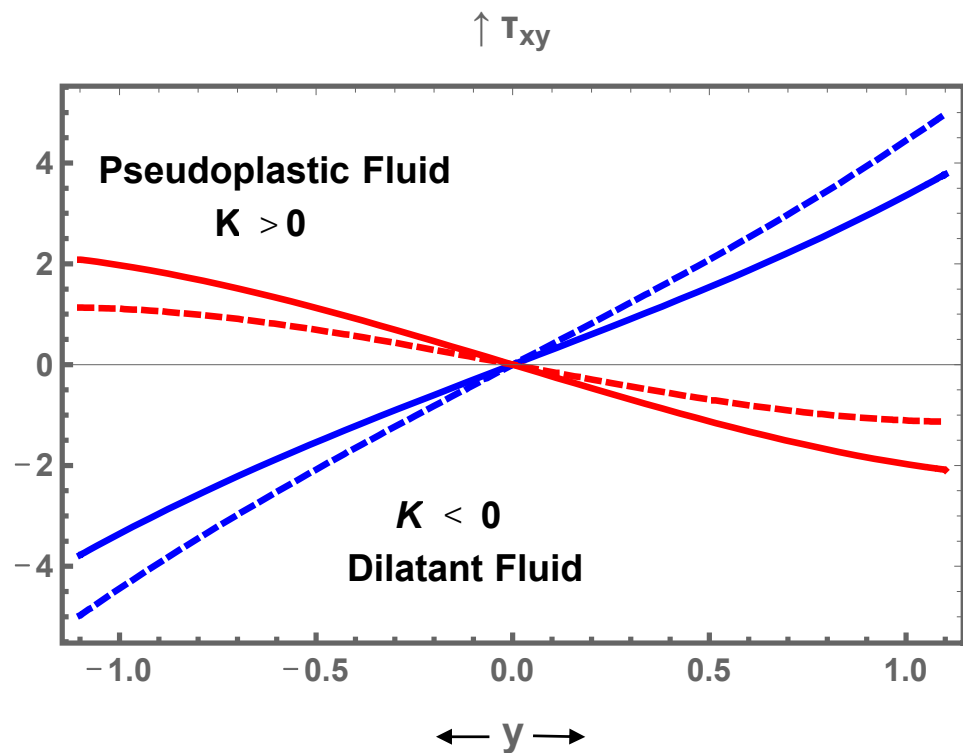


**Figure 9.** Display of shear stress profile via *y* for pseudoplastic and dilatant fluids.
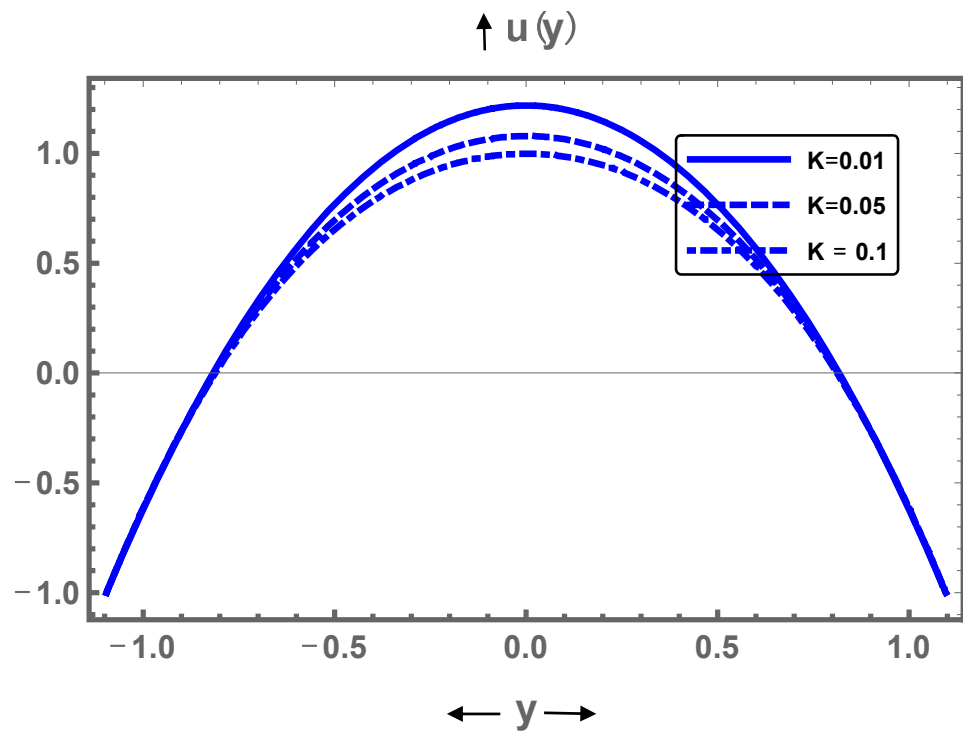
**Figure 10.** Display of axial velocity for different values of $K$.
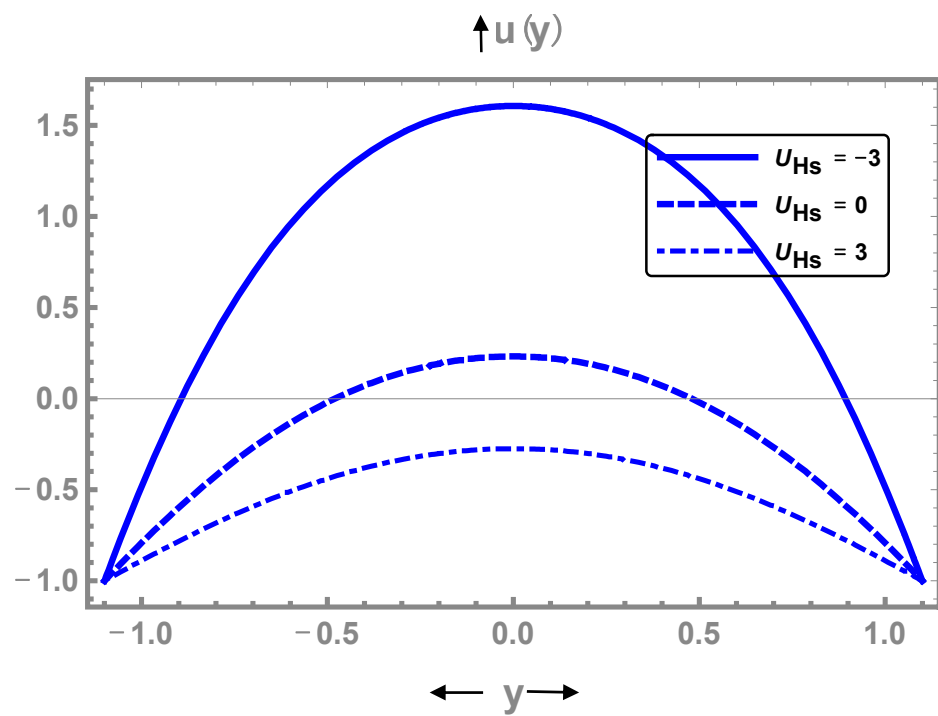


**Figure 11.** Display of axial velocity for different values of $U_{HS}$.
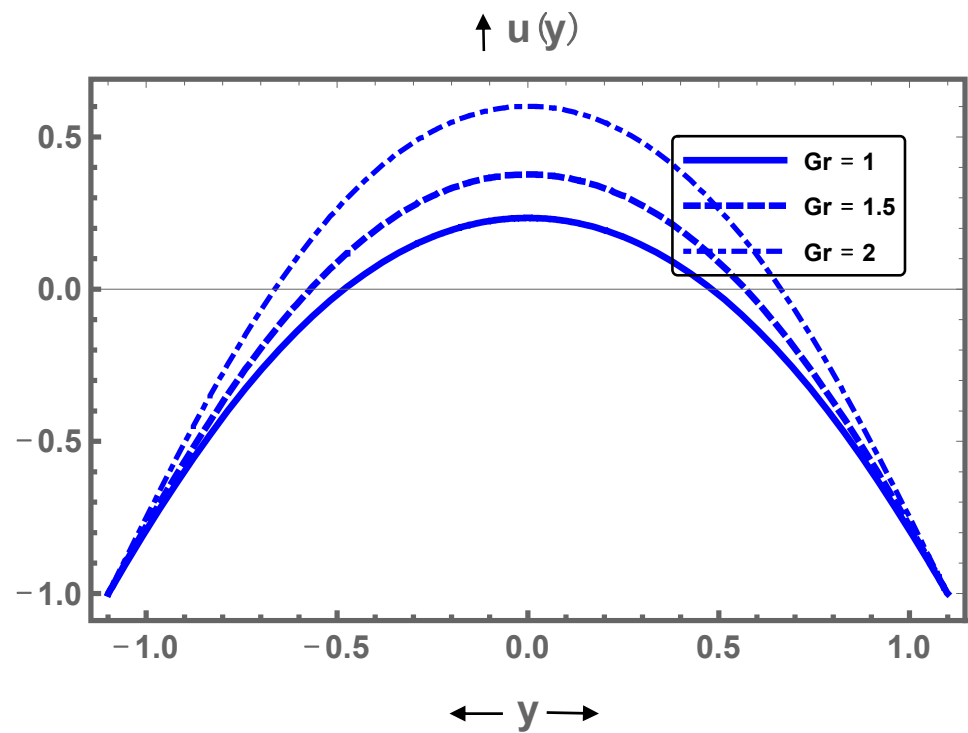
**Figure 12.** Display of axial velocity for different values of *Gr*.
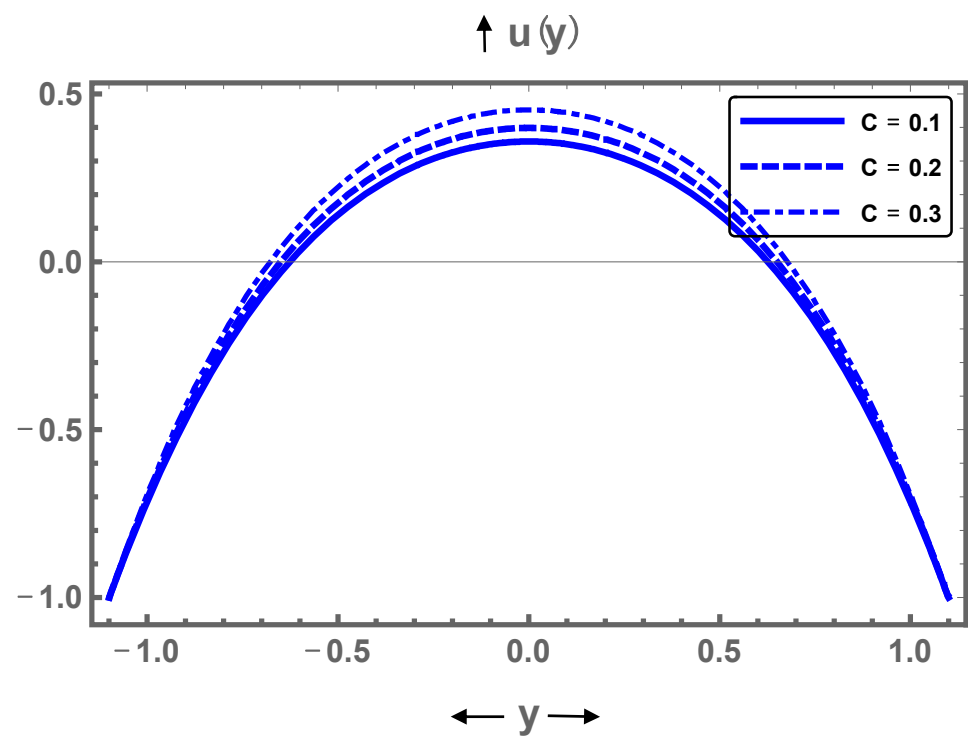


**Figure 13.** Display of axial velocity for different values of *C*.
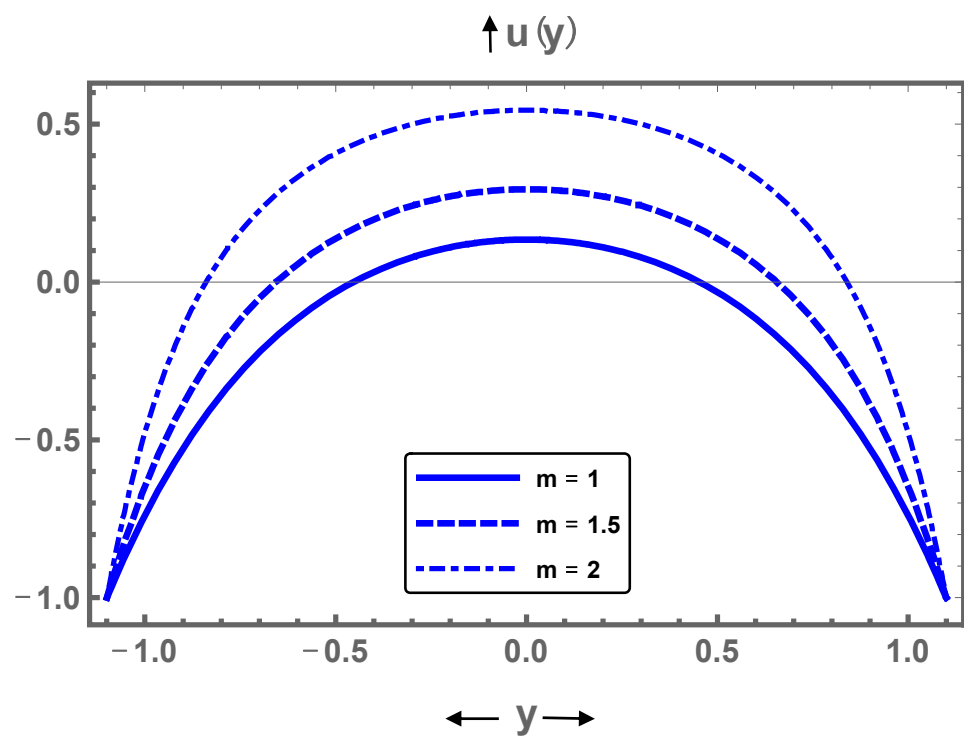
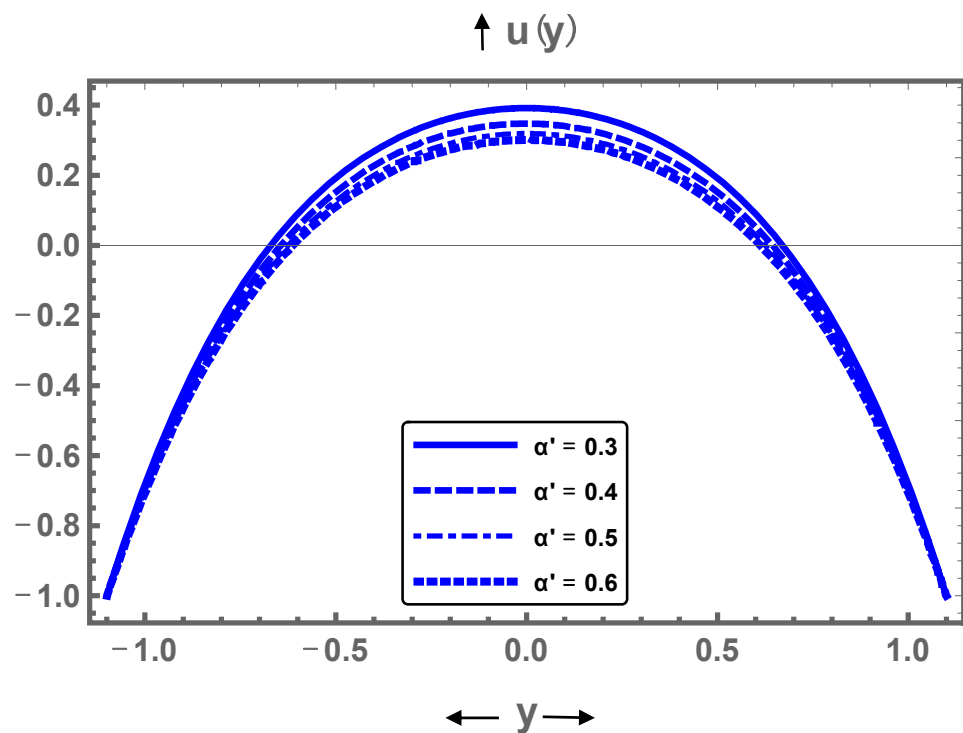**Figure 14.** Display of axial velocity for different values of $m$.



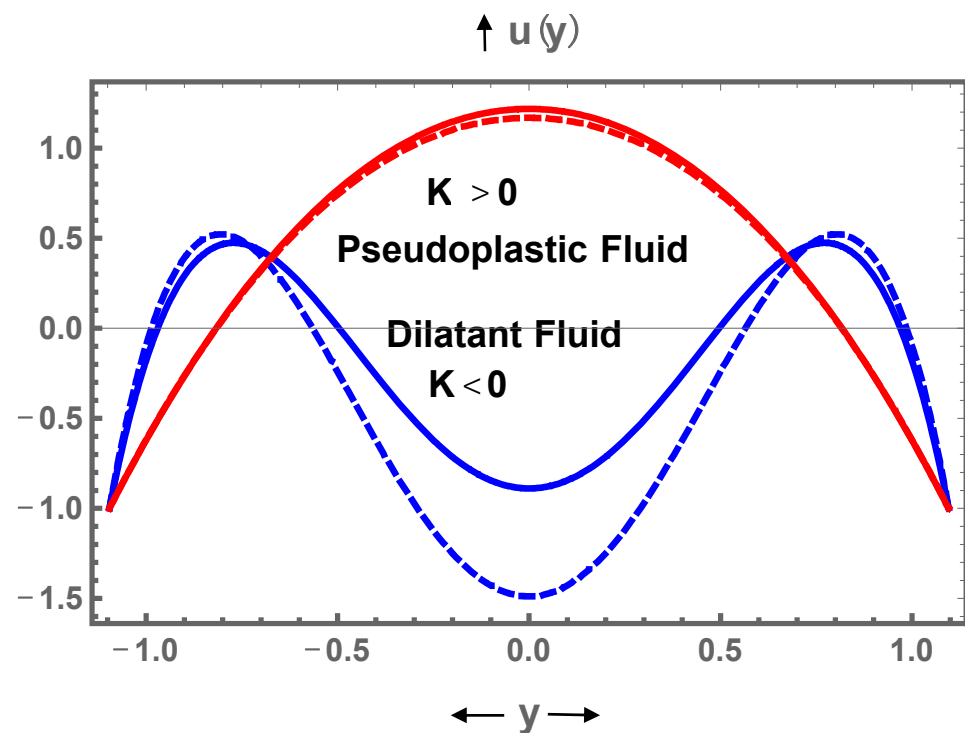**Figure 15.** Display of axial velocity for different values of $\alpha'$.

**Figure 16.** Display of axial velocity for pseudoplastic and dilatant fluids.

Figures 17–22 are prepared in order to see the behaviour of $\frac{dp}{dx}$ along the axis of the conduit under the effect of $K$, $C$, $U_{HS}$, $Gr$, $m$, and $\alpha'$. It is seen that $K$, $C$, $m$, and $\alpha'$ serve to reduce $\frac{dp}{dx}$ for all values of the pertinent parameters, as noticed in Figures 17, 18, 21 and 22. It is also noticed from Figures 19 and 20 that $\frac{dp}{dx}$ grows for greater values of $U_{HS}$ and $Gr$. It is also observed that for $x \in [0, 2]$ and $[3.9, 6]$, the pressure gradient is small and that the large pressure gradient occurs for $x \in [2.1, 4]$.

Figures 23–28 are prepared in order to spot the variation of $\Delta p$ that is portrayed against the dimensionless time-averaged flux across one wavelength, $Q$, for several values of the parameters under consideration. The contributions of $K$, $Gr$, and $m$ for $\Delta p$ are displayed in Figures 23, 25 and 26, where it is noticed that $\Delta p$ decays near the lower wall of the channel and grows afterwards with an increase in the channel curviness. It is also shown from Figures 24 and 27 that $\Delta p$ attains smaller values as the channel curviness increases away from the wall of the conduit. Finally, Figure 28 displays the behaviour of $\Delta p$ in case of dilatation and pseudoplasticity of fluids. It is seen that $\Delta p$ is generally higher for dilated fluids than that of pseudoplastic ones. It is also observed that $\Delta p$ decreases for dilated fluids all the way along, whereas it decreases for pseudoplastic fluids only until a specific value ($Q = 1$) away from the wall from which the behaviour is reversed.
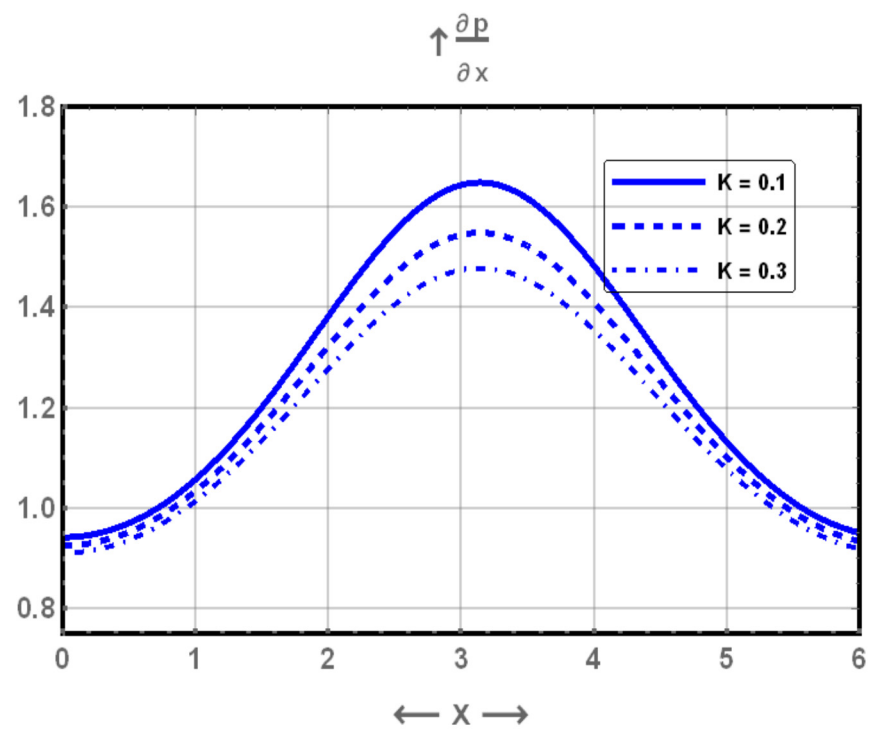
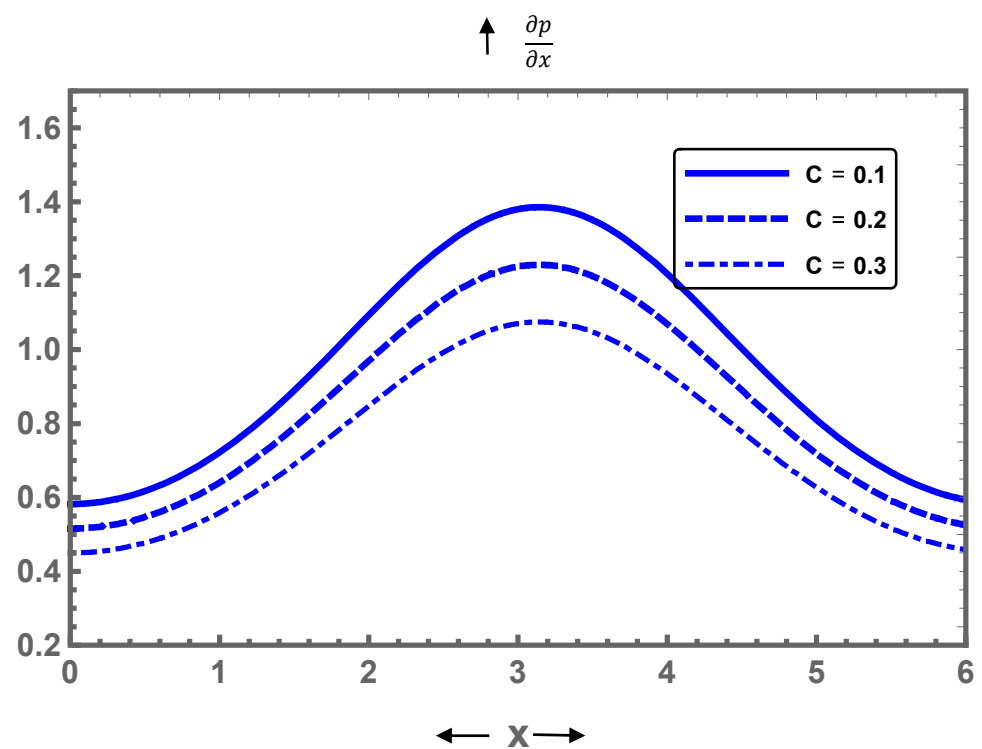**Figure 17.** Display of pressure gradient for different values of *K*.



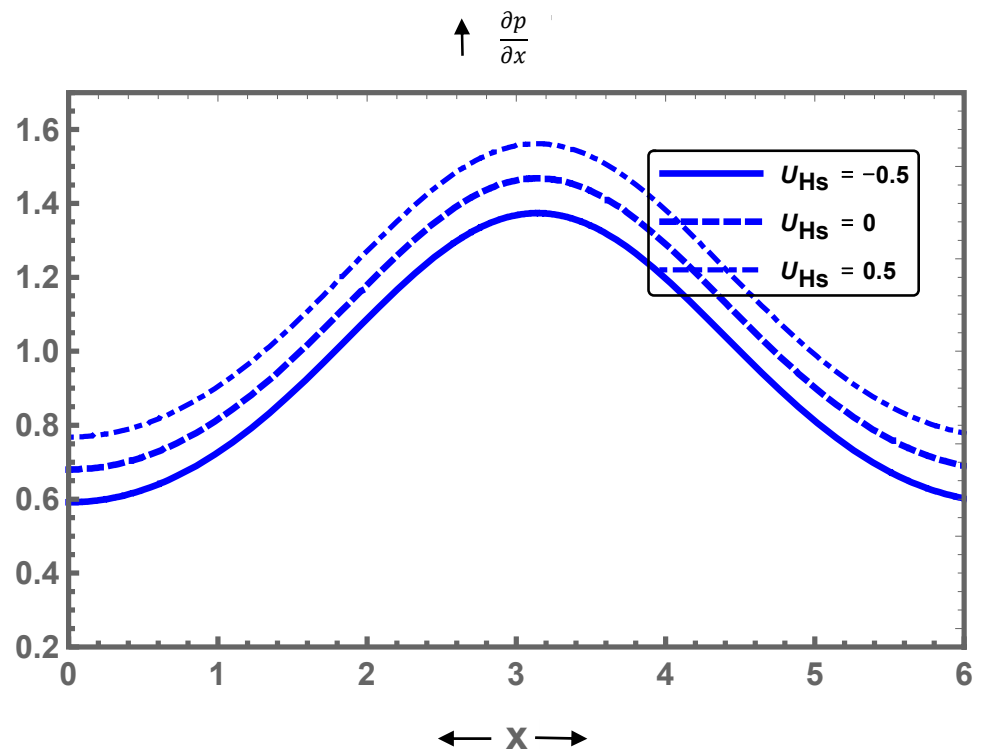**Figure 18.** Display of pressure gradient for different values of *C*.

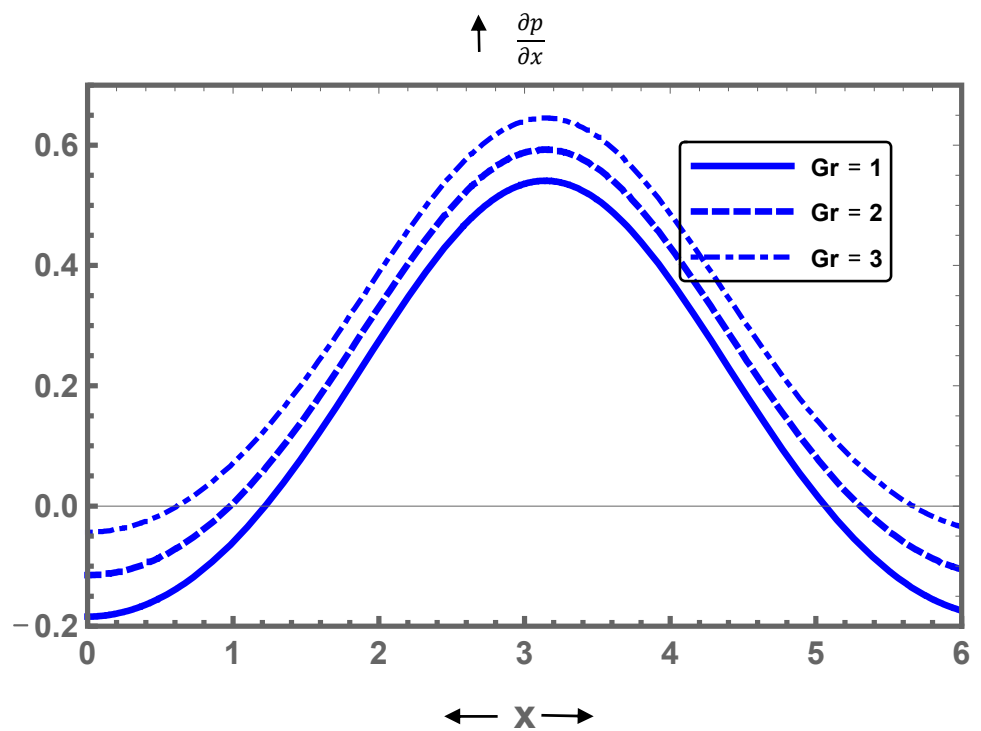**Figure 19.** Display of pressure gradient for different values of $U_{HS}$.



**Figure 20.** Display of pressure gradient for different values of $Gr$.
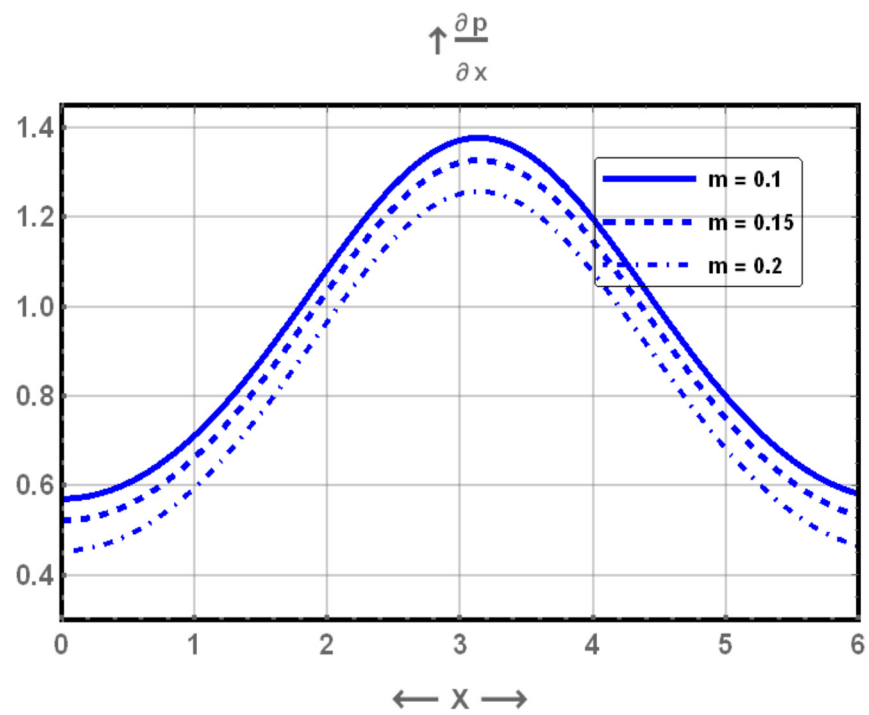
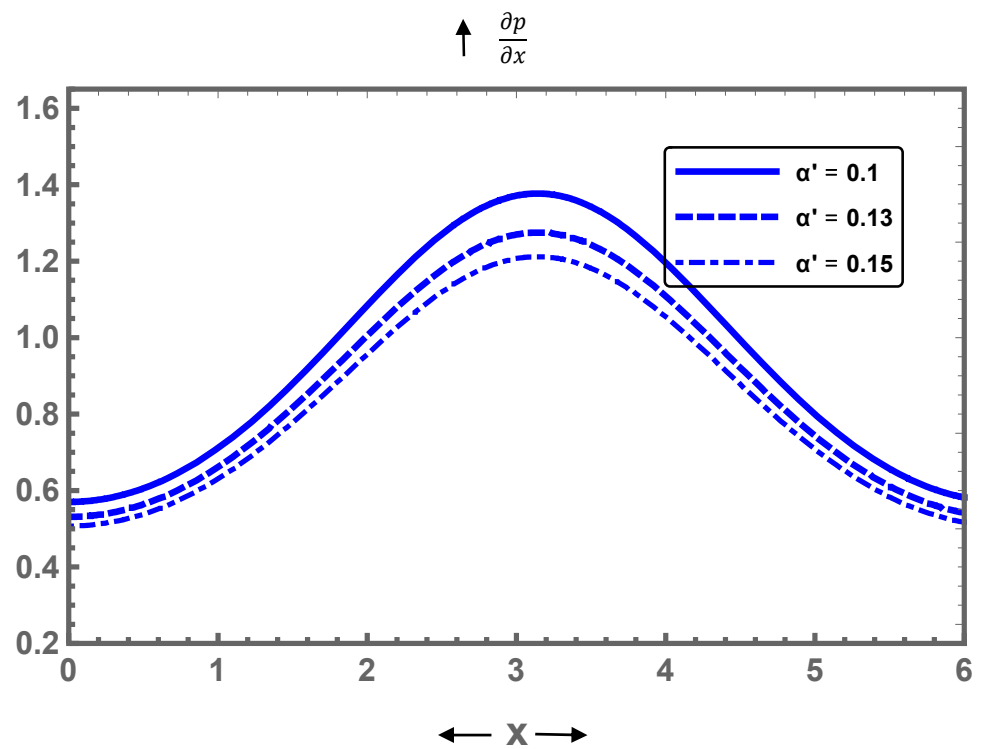**Figure 21.** Display of pressure gradient for different values of *m*.



**Figure 22.** Display of pressure gradient for different values of $\alpha'$.

**Figure 23.** Display of pressure rise vs. volume flow rate for different values of *K*.



**Figure 24.** Display of pressure rise vs. volume flow rate for different values of *C*.

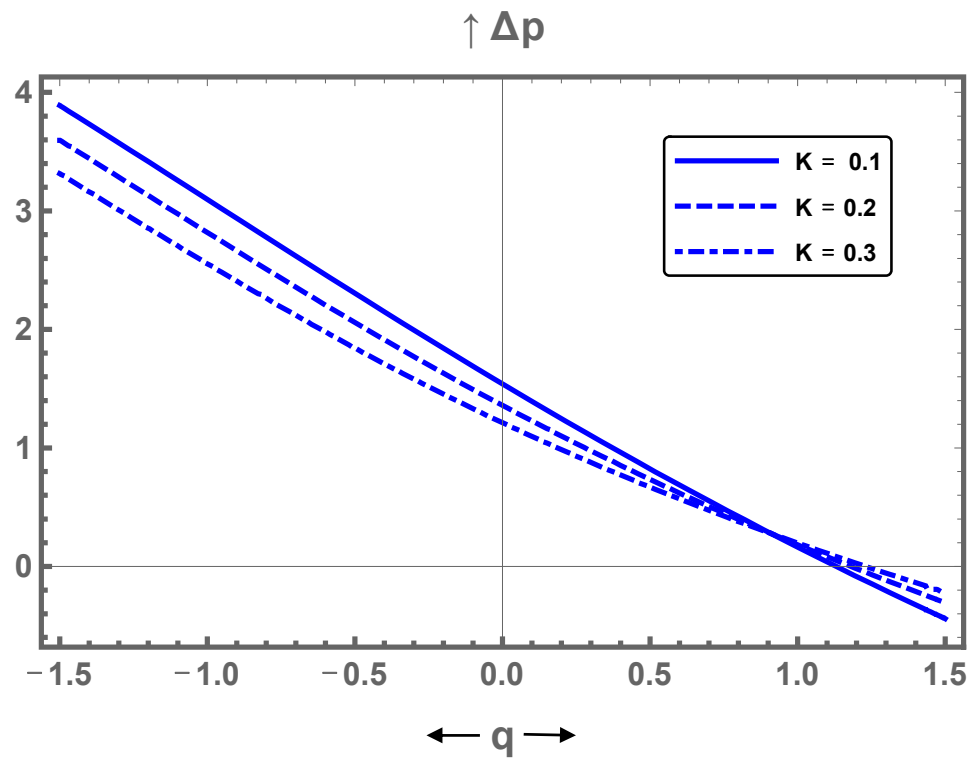**Figure 25.** Display of pressure rise vs. volume flow rate for different values of *Gr*.
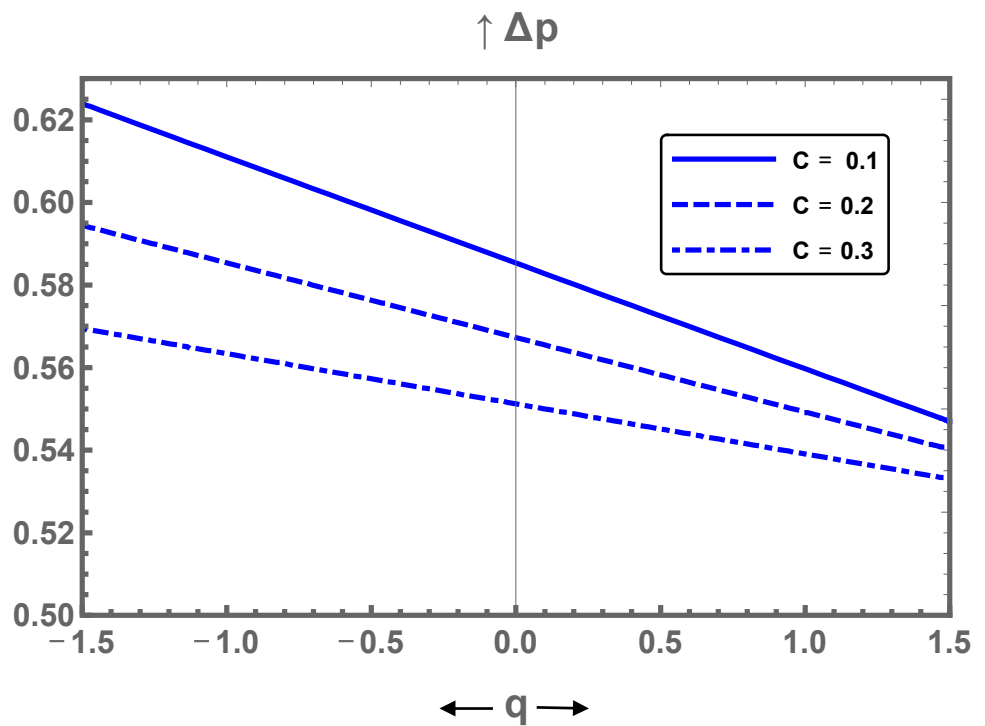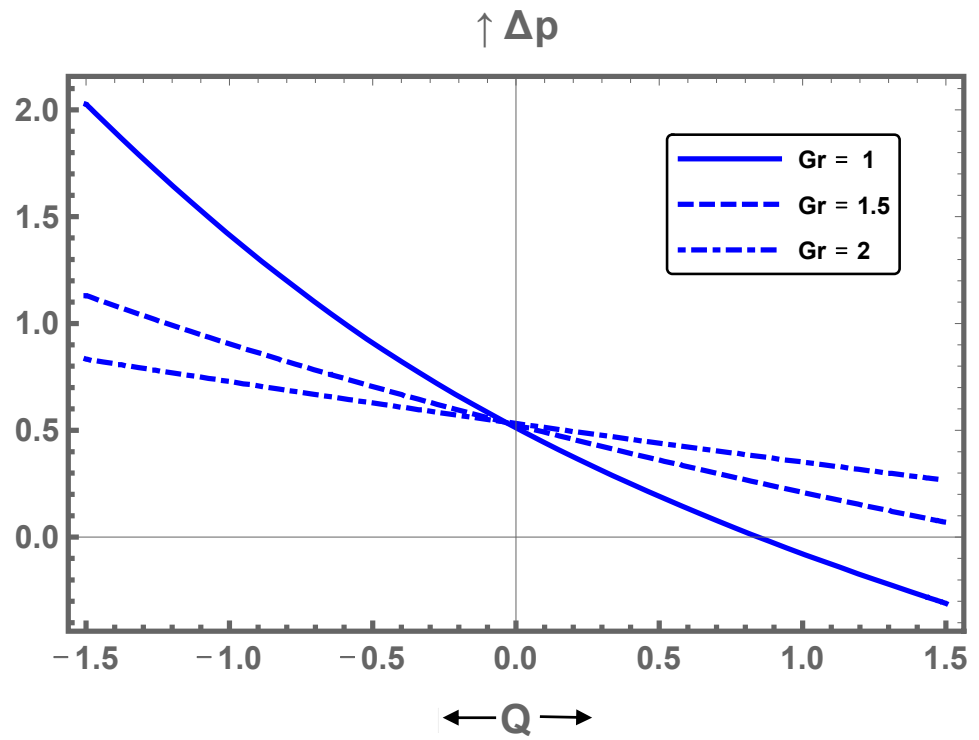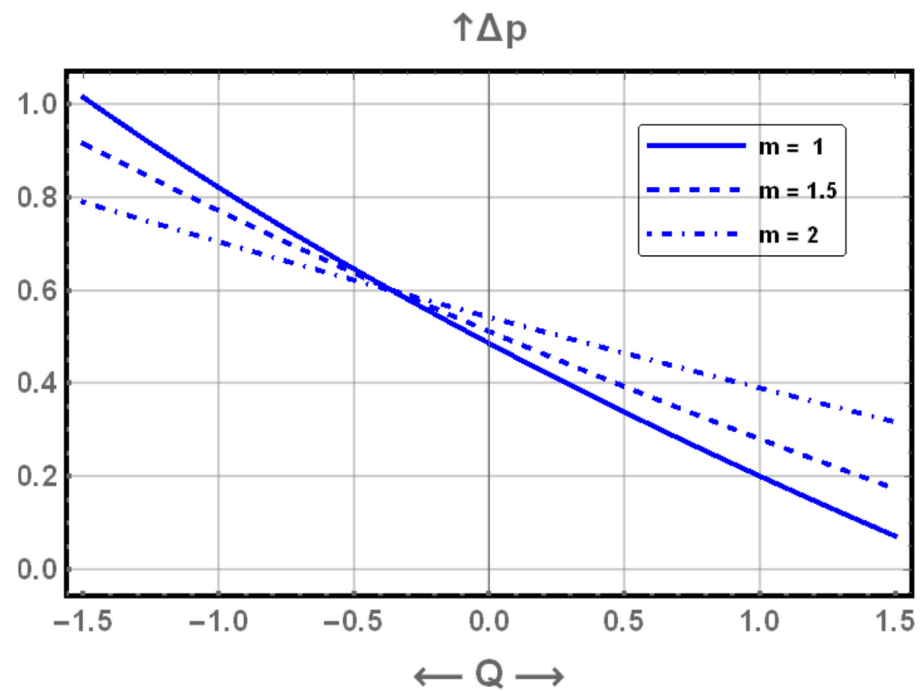


**Figure 26.** Display of pressure rise vs. volume flow rate for different values of *m*.
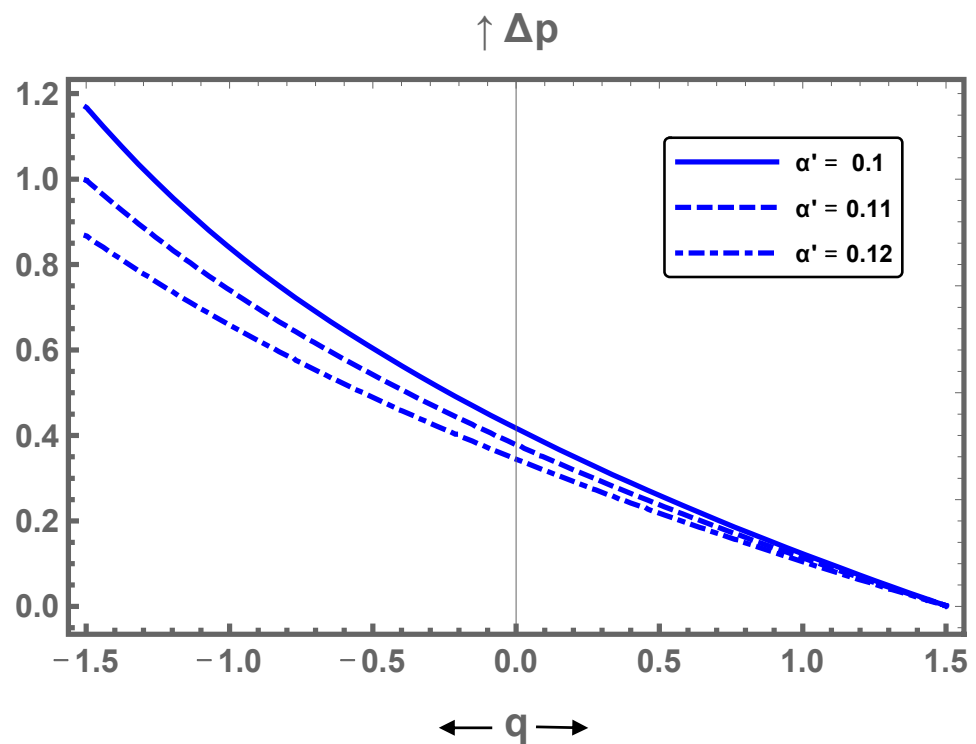
**Figure 27.** Display of pressure rise vs. volume flow rate for different values of $\alpha'$.
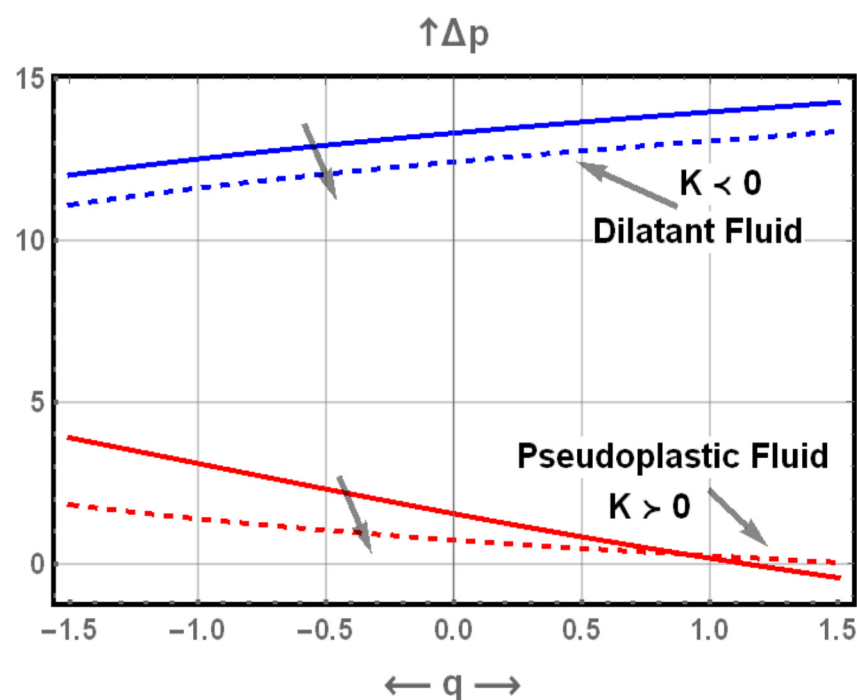


**Figure 28.** Display of pressure rise vs. volume flow rate for pseudoplastic and dilatant fluids.

## 8. Biomedical Application of the Problem

Shear stress of fluid circulation is an important diagnostic aspect for evaluating the properties of blood supply through the arteries. The evolution of shear stress in the consolidated system, combined with the dynamic rheology of the blood, describes the reduction of the circular region of the system over time. Wall shear stress plays a significant part in reshaping the arterial wall, which can contribute to arterial thickening. Table 1 illustrates the non-dimensional shear stresses of Rabinowitsch fluid, $\tau$, through an artery

for various values of the haematocrit, *C*, for diseased blood. It is noticed that as the C increases, $\tau$ increases.

**Table 1.** Rabinowitsch shear stress through an artery for various values *C*.

| *x* | Shear Stress of Rabinowitsch Fluid $\tau$ | | | | | |
|---|---|---|---|---|---|---|
| | *C* = 0.248 | *C* = 0.28 | *C* = 0.426 | *C* = 0.4325 | *C* = 0.4331 | *C* = 0.632 |
| | Hb SS (Sickle Cell) | Plasma Cell Dyscrasias | Normal Blood | Hypertension (Controlled) | Hypertension (Uncontrolled) | Polycythemia |
| 0. | 0.508917 | 0.538364 | 0.707973 | 0.717319 | 0.718192 | 1.15146 |
| 0.2 | 0.505563 | 0.534945 | 0.704064 | 0.713379 | 0.714249 | 1.14586 |
| 0.4 | 0.495578 | 0.524771 | 0.69247 | 0.701695 | 0.702557 | 1.12931 |
| 0.6 | 0.479179 | 0.508091 | 0.673581 | 0.682663 | 0.683511 | 1.10248 |
| 0.8 | 0.456697 | 0.485281 | 0.64801 | 0.656909 | 0.657739 | 1.0665 |
| 1. | 0.428523 | 0.456801 | 0.616547 | 0.625236 | 0.626047 | 1.02282 |
| 1.2 | 0.395056 | 0.423142 | 0.580099 | 0.588575 | 0.589366 | 0.973144 |
| 1.4 | 0.35665 | 0.384766 | 0.539639 | 0.54792 | 0.548692 | 0.919356 |
| 1.6 | 0.313594 | 0.34209 | 0.496165 | 0.504294 | 0.505052 | 0.86342 |
| 1.8 | 0.266209 | 0.295542 | 0.450704 | 0.458753 | 0.459502 | 0.807327 |
| 2. | 0.215192 | 0.245805 | 0.404386 | 0.41245 | 0.4132 | 0.753059 |
| 2.2 | 0.162415 | 0.194396 | 0.358613 | 0.3668 | 0.367561 | 0.702604 |
| 2.4 | 0.111854 | 0.144497 | 0.315318 | 0.323729 | 0.324509 | 0.657972 |
| 2.6 | 0.0690173 | 0.101038 | 0.277209 | 0.285898 | 0.286704 | 0.621209 |
| 2.8 | 0.038254 | 0.0688821 | 0.24769 | 0.256637 | 0.257466 | 0.594302 |
| 3. | 0.0213037 | 0.0508044 | 0.23019 | 0.2393 | 0.240144 | 0.578956 |
| 3.2 | 0.0183903 | 0.0476728 | 0.227071 | 0.236211 | 0.237058 | 0.576266 |
| 3.4 | 0.029497 | 0.0595737 | 0.238779 | 0.247809 | 0.248646 | 0.586434 |
| 3.6 | 0.0546015 | 0.0860756 | 0.26368 | 0.272484 | 0.2733 | 0.608713 |
| 3.8 | 0.0927918 | 0.125329 | 0.298654 | 0.307178 | 0.307969 | 0.641609 |
| 4. | 0.140811 | 0.173205 | 0.340168 | 0.348438 | 0.349206 | 0.683216 |
| 4.2 | 0.19328 | 0.22449 | 0.385186 | 0.393288 | 0.394041 | 0.731496 |
| 4.4 | 0.245362 | 0.275183 | 0.431472 | 0.439514 | 0.440263 | 0.78442 |
| 4.6 | 0.294386 | 0.323171 | 0.477437 | 0.485523 | 0.486276 | 0.839995 |
| 4.8 | 0.339291 | 0.367516 | 0.521865 | 0.530076 | 0.530841 | 0.896238 |
| 5. | 0.379664 | 0.407729 | 0.563701 | 0.572092 | 0.572875 | 0.95116 |

## 9. Deductions

In this article, the impact of Rabinowitsch suspension fluid through elastic walls with heat transfer under the effect of the electroosmotic forces is investigated. The solutions of the fluid model are achieved by taking a long wavelength approximation. A comparison is set between the effect of pseudoplasticity and dilatation on the behaviour of shear stress, axial velocity, and pressure rise. The impact of all the pertinent parameters are discussed graphically. The main observations are as follows:

i.      Unlike the effect of the radius of the channel for elasticity on the shear stress, it tends to reduce the axial velocity, pressure gradient, and pressure rise.

ii.     The volume fraction boosts the shear stress and the axial velocity, whereas the effect is totally reversed with the pressure gradient and pressure rise.

   iii.    The Grashof number accelerates the flow and increases shear stresses along with the pressure gradient.

   iv.    The maximum axial velocity takes place at the centre of the conduit.

   v.    The maximum electroosmotic velocity boosts the shear stress and pressure gradient but reduces the axial velocity.

   vi.    The influence of the Rabinowitsch and electroosmotic parameters is to enhance the shear stress, whereas their effect is totally reversed for the pressure gradient.

   vii.    The current model reduces to the case of dilatant fluid for $K < 0$, pseudoplastic fluid for $K > 0$.

**Author Contributions:** Conceptualization, S.I.A.; methodology, A.Z.Z.; software, A.Z.Z.; validation, S.I.A.; formal analysis, A.Z.Z.; investigation, S.I.A.; resources, A.Z.Z.; data curation, S.I.A. and A.Z.Z.; writing—original draft preparation, S.I.A. and A.Z.Z.; writing—review and editing, S.I.A.; visualization, A.Z.Z.; supervision, S.I.A.; project administration, S.I.A. All authors have read and agreed to the published version of the manuscript.

## Appendix A

The constants given in Equations (32), (33) and (36) are defined as:

$$P = \frac{dp}{dx}.$$

$$P_1(y) = 6P + QG_r(-3h^2 + y^2).$$

$$P_2(y) = 2P + QG_r(-h^2 + y^2).$$

$$P_3(y) = 12P + QG_r(-6h^2 + 5y^2).$$

$$P_4(y) = -4P + QG_r(2h^2 - 5y^2).$$

$$c_0 = \frac{1}{8640\,\overline{\mu}\,m^6 C_{PH}^3}.$$

$$
\begin{aligned}
c_1 = m^6 (&-8640\,\overline{\mu}\;C_{PH}^3 \\
&+h^2(540Km^2 U_{Hs}{}^2 Sech^2(hm)(12P - 5h^2 QG_r) \\
&+360C_{PH}^2(-12P + 5h^2 QG_r) \\
&+h^2 K(-2160(P)^3 + 2520h^2 QG_r(P)^2 \\
&-990h^4 Q^2 G_r^2 P + 131h^6 Q^3 G_r^3)) \\
&+90y^4(4QC_{PH}^2 G_r \\
&+3K(-2m^2 QUhs^2 Sech^2(hm)G_r \\
&+(2P - h^2 QG_r)^3))).
\end{aligned}
$$

$$c_2 = 4\,Km^6\,Q^3\;G_r^3.$$

$$c_3 = 1080\,m^6\,(-3Km^2 U_{Hs}{}^2 Sech^2(h(x)m) + 2C_{PH}^2)(2P - h^2 QG_r).$$

$$c_4 = -45\,Km^6\,Q^2 G_r^2(-2P + h^2 QG_r).$$

$$c_5 = 180\,K\,m^6\,Q\,G_r(-2P + h^2 QG_r)^2.$$

$$c_6 = -720\,K\,m^8\,U_{HS}{}^3\,Sech^3(hm).$$

$$c_7 = 1620\,K\,m^5\,U_{HS}{}^2\;Q\,G_r\,Sech^2(hm).$$

$$c_8 = 180\,m^2\,U_{HS}\,Sech(hm).$$

$$c_9 = c_{11} Q\,G_r$$

$$c_{10} = 2m^2 c_{11}.$$

$$c_{11} = -810\,K\,m^4\,U_{HS}{}^2\,Sech^2(hm).$$

$$c_{12} = c_{15}\, m^4.$$
$$c_{13} = 4m^2 Q\, G_r\, c_{15}.$$
$$c_{14} = 90\, U_{HS}\, m^6 K\, Sech(hm).$$
$$c_{15} = 4320\, K\, m\, U_{HS}\, Sech(hm).$$
$$c_{16} = 120\, Q^2\, G_r^2.$$
$$\begin{aligned}
c_{17} = & -720\, U_{HS}\, (9Km^8 U_{HS}{}^2 Sech^2(hm)+ \\
& 4(-9Km^4(2+h^2 m^2)(P)^2 - 3m^6 C_{PH}^2 + \\
& 6Km^2(-12-3h^2 m^2 + h^4 m^4)QG_r P - K(180+ \\
& 54h^2 m^2 - 6h^4 m^4 + h^6 m^6)Q^2 G_r^2)) \\
& Km(8m^7 U_{HS}{}^2 Cosh(3hm)Sech^2(hm)+) \\
& 9m^3 U_{HS}\, Cosh(2hm)Sech(hm)(4m^2 P + QG_r)+ \\
& 6h(m^4 U_{HS}\, Sech(hm)\, Sinh(2hm)(-12\, m^2 P+ \\
& (-3+4h^2 m^2)QG_r) + 32\sinh(hm)(-3m^4 P^2 + \\
& m^2(-12+h^2 m^2)QG_r P + (-30+h^2 m^2)Q^2 G_r^2))).
\end{aligned}$$
$$c_{18} = 90\, U_{HS}\, Sech(hm)(9Km^8 U_{HS}{}^2 Sech^2(hm) - 720KQ^2 G_r^2) + c22.$$
$$c_{19} = 6480\, Km^2 QG_r\, U_{HS}\, Sech(hm).$$
$$c_{20} = -2700\, Q^2\, G_r^2\, m^4\, K\, U_{HS}\, Sech(hm).$$
$$c_{21} = 1080\, Q\, G_r(-2P + h^2 QG_r)\, U_{HS}\, Sech(hm)6Km^4.$$
$$c_{22} = 1620\, K\, m^4\, U_{HS}\, (-2P + h^2 QG_r)^2\, Sech(hm).$$
$$c_{23} = -1080\, C_{PH}^2\, m^6\, U_{HS}\, Sech(hm).$$

$$\begin{aligned}
c_{24} = \frac{1}{8640\overline{\mu}m^6 M^3}\Big\{ & -8640\, \overline{\mu}\, h(x)m^6 M^3 + 1152\, G_r\, h(x)^5 m^6 M^2 Q \\
& + \frac{7552}{77} G_r{}^3 h(x)^{11} K\, m^6\, Q^3 - 1728c1^2 G_r\, h(x)^5 K\, m^8\, Q\, U_{HS}{}^2 + \\
& 8640\, h(x)\, m^6 M^2 U_{HS} + 1555200\, G_r{}^2 h(x)\, K\, Q^2 U_{HS} - \\
& 34560 G_r{}^2 h(x)^3 Km^2 Q^2 U_{HS} - 34560 G_r{}^2 h(x)\, K(-45+h^2 m^2)\, Q^2 U_{HS} + \\
& 2880\, G_r{}^2 h(x)\, K(180 + 54h(x)^2 m^2 - 6h(x)^4 m^4 + h(x)^6 m^6)\, Q^2 U_{HS} - \\
& 6480 h(x)\, K\, m^8 U_{HS}{}^3\, sech^2(h(x)\, m) + \\
& 3240 G_r h(x) Km^4 Q U_{HS}{}^2 cosh(2h(x)m)sech^2(h(x)m) - \\
& 1080 G_r h(x)^3 Km^6 Q U_{HS}{}^2 cosh(2h(x)m)sech^2(hm) + \\
& 720\, h(x) Km^8 U_{HS}{}^3 cosh(3h(x)m)sech^3(h(x)m) - \\
& 8640\, m^5 M^2 U_{HS} tanh(h(x)m) - \frac{2073600\, G_r{}^2 KQ^2 Uhstanh(h(x)m)}{m} - \\
& 466560\, G_r{}^2 h(x)^2 KmQ^2 U_{HS} tanh(h(x)m) + \\
& G_r{}^2 h(x)^4 Km^3 Q^2 U_{HS} tanh(h(x)m)(34560 - 2880 G_r{}^2 h(x)^2 m^2) + \\
& 17280\, G_r{}^2 h(x)^2 Km(-30 + h(x)^2 m^2)\, Q^2 U_{HS} tanh(h(x)m) - \\
& \frac{17280\, G_r{}^2 K(90+18h(x)^2 m^2 - h(x)^4 m^4)Q^2 U_{HS} tanh(h(x)m)}{m} + \\
& 6480\, Km^7 U_{HS}{}^3 tanh(h(x)m)\, sech^2(h(x)m) - \\
& 1620\, G_r Km^3 Q U_{HS}{}^2 tanh(h(x)m) - 1620\, G_r h(x)^2\, Km^5 Q U_{HS}{}^2 tanh(h(x)m) + \\
& 2160\, G_r h(x)^4 Km^7 Q U_{HS}{}^2 tanh(h(x)m) - \\
& 240\, Km^7 U_{HS}{}^3 sinh(3h(x)m)sech^3(h(x)m)\Big\}.
\end{aligned}$$

## References

1. SherAkbar, N.; WahidButt, A. Heat transfer analysis of Rabinowitsch fluid flow due to metachronal wave of cilia. *Results Phys.* **2015**, *5*, 92–98.
2. Singh, B.K.; Singh, U.P. Analysis of peristaltic flow in a tube: Rabinowitsch fluid model. *Int. J. Fluids Eng.* **2014**, *6*, 1–8.
3. Vaidya, H.; Rajashekhar, C.; Manjunatha, G.; Prasad, K.V. Peristaltic mechanism of a Rabinowitsch fluid in an inclined channel with complaint wall; variable liquid properties. *J. Braz. Soc. Mech. Sci. Eng.* **2019**, *41*, 52. [CrossRef]
4. Sadaf, H.; Nadeem, S. Analysis of combined convective and viscous dissipation effects for peristaltic flow of Rabinowitsch fluid model. *J. Bionic Eng.* **2017**, *14*, 182–190. [CrossRef]
5. Choudhari, R. Analysis of peristaltic flow of Rabinowitsch fluid in a non-uniform channel: Analytical approach. *Lat. Am. Appl. Res.* **2020**, *50*, 151–158.
6. Mekheimer, K.; Zaher, A.; Hasona, W. Entropy of AC electro-kinetics for blood mediated gold or copper nanoparticles as a drug agent for thermotherapy of oncology. *Chin. J. Phys.* **2020**, *65*, 123–138. [CrossRef]
7. Mekheimer, K.S.; Zaher, A.Z.; Abo-Elkhair, R.E. Electro-magnetohydrodynamic oscillatory flow of a dielectric fluid through a porous medium with heat transfer: Brinkman model. *Bionanoscience* **2018**, *8*, 596–608.

8.      Zaher, A.; Ali, K.K.; Mekheimer, K.S. Electroosmosis forces EOF driven boundary layer flow for a non-newtonian fluid with planktonic microorganism: Darcy Forchheimer model. *Int. J. Numer. Methods Heat Fluid Flow* **2021**, *31*, 2534–2559. [CrossRef]

9.      Reuss, F.F. *Mémoires de la Société Impériale des Naturalistes de Moscou*; Imperial Moscow University: Moscow, Russian, 1809; Volume 2, pp. 327–337.

10.    Mekheimer, K.S.; Zaher, A.; Abdellateef, A.I. Entropy hemodynamics particle-fluid suspension model through eccentric catheterization for time-variant stenotic arterial wall: Catheter injection. *Int. J. Geom. Methods Mod. Phys.* **2019**, *16*, 164–496. [CrossRef]

11.    Zeeshan, A.; Ijaz, N.; Bhatti, M.M. Flow analysis of particulate suspension on an asymmetric peristaltic motion in a curved configuration with heat and mass transfer. *Mech. Ind.* **2018**, *19*, 401. [CrossRef]

12.    Abdelsalam, S.I.; Vafai, K. Particulate suspension effect on peristaltically induced unsteady pulsatile flow in a narrow artery: Blood flow model. *Math. Biosci.* **2017**, *283*, 91–105. [CrossRef]

13.    Khan, A.A.; Tariq, H. Influence of wall properties on the peristaltic flow of a dusty Walter's B fluid. *J. Braz. Soc. Mech. Sci. Eng.* **2018**, *40*, 368. [CrossRef]

14.    Choi, S.U.S.; Eastman, J.A. Enhancing thermal conductivity of fluids with nanoparticles. In *Developments and Applications of Non-Newtonian Flows*; Siginer, D.A., Wang, H.P., Eds.; ASME: New York, NY, USA, 1995; pp. 99–105.

15.    Sadaf, H.; Abdelsalam, S.I. Adverse effects of hybrid nanofluid in a wavy nonuniform annulus with convective boundary conditions. *RSC Adv.* **2019**, *10*, 15035–15043. [CrossRef]

16.    Bhatti, M.M.; Ellahi, R.; Zeeshan, A.; Marin, M.; Abdelsalam, S.I. Swimming of motile gyrotactic microorganisms and movement of nanoparticles in blood flow through anisotropically tapered arteries. *Front. Phys.* **2020**, *8*, 1–9. [CrossRef]

17.    Abdelsalam, S.I.; Bhatti, M.M. Anomalous reactivity of thermo-bioconvective nanofluid towards oxytactic microorganisms. *Appl. Math. Mech.* **2020**, *41*, 1–14. [CrossRef]

18.    Mekheimer, K.; Hasona, W.; Abo-Elkhair, R.; Zaher, A. Peristaltic blood flow with gold nanoparticles as a third grade nanofluid in catheter: Application of cancer therapy. *Phys. Lett. A* **2018**, *382*, 85–93. [CrossRef]

19.    Sohail, M.; Naz, R.; Abdelsalam, S.I. On the onset of entropy generation for a nanofluid with thermal radiation and gyrotactic microorganisms through 3D flows. *Phys. Scr.* **2020**, *95*, 045206. [CrossRef]

20.    Abdelsalam, S.I.; Bhatti, M.M. The study of non-newtonian nanofluid with hall and ion slip effects on peristaltically induced motion in a non-uniform channel. *RSC Adv.* **2018**, *8*, 7904–7915. [CrossRef]

21.    Nguyen-Thoi, T.; Sheikholeslami, M.; Hamid, M.; Haq, R.-U.; Shafee, A. CVFEM modeling for nanofluid behavior involving non-equilibrium model and Lorentz effect in appearance of radiation. *Phys. A Stat. Mech. Appl.* **2019**, *534*. [CrossRef]

22.    Khan, Z.H.; Usman, M.; Zubair, T.; Hamid, M.; Haq, R.U. Brownian motion and thermophoresis effects on unsteady stagnation point flow of eyring–powell nanofluid: A Galerkin approach. *Commun. Theor. Phys.* **2020**, *72*, 125005. [CrossRef]

23.    Khan, Z.H.; Khan, W.A.; Haq, R.; Usman, M.; Hamid, M. Effects of volume fraction on water-based carbon nanotubes flow in a right-angle trapezoidal cavity: FEM based analysis. *Int. Commun. Heat Mass Transf.* **2020**, *116*, 104640. [CrossRef]

24.    Khan, Z.H.; Khan, W.A.; Hamid, M.; Liu, H. Finite element analysis of hybrid nanofluid flow and heat transfer in a split lid driven square cavity with Y-shaped obstacle. *Phys. Fluids* **2020**, *32*, 093609. [CrossRef]

25.    Sochi, T. The flow of Newtonian and power law fluids in elastic tubes. *Int. J. Non-Linear Mech.* **2014**, *67*, 245–250. [CrossRef]

26.    Sarkar, A.; Jayaraman, G. Non-linear analysis of oscillatory flow in the annulus of an elastic tube: Application to catheterized artery. *Phys. Fluids* **2001**, *13*, 2901–2911. [CrossRef]

27.    Pedrizzetti, G. Fluid flow in a tube with an elastic membrane insertion. *J. Fluid Mech.* **1998**, *375*, 39–64. [CrossRef]

28.    Rubinow, S.I.; Keller, J.B. Flow of a viscous fluid through an elastic tube with applications to blood flow. *J. Theor. Biol.* **1972**, *35*, 299–313. [CrossRef]

29.    Marin, M.; Ellahi, R.; Chirila, A. On solutions of Saint-Venant's problem for elastic dipolar bodies with voids. *Carpathian J. Math.* **2017**, *33*, 219–232. [CrossRef]

30.    Marin, M.; Ellahi, R.; Vlase, S.; Bhatti, M.M. On the decay of exponential type for the solutions in a dipolar elastic body. *J. Taibah Univ. Sci.* **2020**, *14*, 534–540. [CrossRef]

31.    Marin, M.; Öchsner, A.; Ellahi, R.; Bhatti, M.M. A semigroup of contractions in elasticity of porous bodies. *Contin. Mech. Thermodyn.* **2021**, *33*, 2027–2037. [CrossRef]

32.    Ijaz, N.; Zeeshan, A.; Bhatti, M. Peristaltic propulsion of particulate non-newtonian Ree-eyring fluid in a duct through constant magnetic field. *Alex. Eng. J.* **2018**, *57*, 1055–1060. [CrossRef]